The Half-Space Matching method for elastodynamic scattering problems in unbounded domains

Éliane Bécache, Anne-Sophie Bonnet-Ben Dhia, Sonia Fliss, Antoine Tonnoir

The Half-Space Matching method for elastodynamic scattering problems in unbounded domains

Éliane Bécache[a], Anne-Sophie Bonnet-Ben Dhia[a], Sonia Fliss[a], Antoine Tonnoir[b]

[a] *POEMS (UMR 7231 CNRS-ENSTA-INRIA), Université Paris Saclay ENSTA, 828 Boulevard des Marechaux, 91762 Palaiseau Cedex, France*
[b] *Normandie University, INSA Rouen Normandie, LMI, 76000 Rouen, France*

Abstract

In this paper, the Half-Space Matching (HSM) method, first introduced for scalar problems, is extended to elastodynamics, to solve time-harmonic 2D scattering problems, in locally perturbed infinite anisotropic homogeneous media. The HSM formulation couples a variational formulation around the perturbations with Fourier integral representations of the outgoing solution in four overlapping half-spaces. These integral representations involve outgoing plane waves, selected according to their group velocity, and evanescent waves. Numerically, the HSM method consists in a finite element discretization of the HSM formulation, together with an approximation of the Fourier integrals. Numerical results, validating the method, are presented for different materials, isotropic and anisotropic. Comparisons with the Perfectly Matched Layers (PML) method are performed for several anisotropic materials. These results highlight the robustness of the HSM method compared to the sensitivity of the PML method with respect to its parameters.

Keywords: Anisotropic elastic waves, plane wave representation, Fourier Transform, integral operators.

1. Introduction

In this paper we are interested in frequency-domain elastic wave scattering problems set in homogeneous anisotropic media which are unbounded in all directions. Anisotropic elastic materials appear in many situations. In geophysical applications for seismic exploration, anisotropic behaviors often arise as effective models for isotropic layered media or for isotropic media including fractures [33, 86, 32, 88]. More generally, homogenization of isotropic heterogeneous media (for instance composite materials) leads to anisotropic effective behavior laws [85, 8]. Imaging defects in composite structures using Non-Destructive Testing (NDT) is another important field of applications, for instance in austenitic stainless steel materials. In all these applications, the propagation domain is often very large compared to the size of the scatterer(s) and to the characteristic wavelength, so that it is relevant to consider the domain as unbounded.

The need for efficient numerical methods to take into account the unbounded character of the domain is crucial to get accurate and reliable results. Even if it is an old and classical question, addressed since

the 1980s for various propagation models (acoustics, electromagnetics, elastodynamics etc), it remains challenging especially in elastodynamics. This motivates the present paper. In general, the principle of these numerical methods is to truncate the domain to a region of interest, while taking into account outgoing waves which propagate towards infinity, without introducing spurious reflections inside the computational domain. Several families of *local* and *non-local* methods have been proposed in the literature in the time-domain as well as in the frequency-domain.

The first historical *local* methods, appeared in the early 1980s, are Absorbing Boundary Conditions (ABCs), initially designed for the transient scalar wave equation and then extended to other time-dependent or time-harmonic models. They consist in introducing an artificial boundary to truncate the computational domain and in setting on this boundary local approximations of the Dirichlet-to-Neumann (DtN) operator, involving only differential operators (e.g. [50, 51, 12, 66, 67, 60, 57, 39]). Besides, in the 1990's, Perfectly Matched Layers (PMLs), another family of local methods based on domain truncation by an absorbing layer, became very popular. Introduced originally for time-dependent Maxwell's equations by Bérenger [18], they have been rapidly extended to other models (see below). These two families of methods are well suited to numerical schemes based on volume methods such as finite differences, finite elements or Discontinuous Galerkin methods.

For the *isotropic scalar* wave equation, ABCs and PMLs are now well analysed in the time-domain (e.g. [50, 51, 12, 66, 67, 59, 60, 57, 39, 56, 47] for ABCs, [1, 48, 7, 16, 2, 17] for PMLs) as well as in the frequency-domain i.e. for the Helmholtz equation (e.g. [69, 98, 82] for ABCs, [76, 19, 27, 28, 70, 62, 83] for PMLs). Direct extensions of these methods to other scalar models may fail in presence of anisotropy but roughly speaking, there have been new solutions designed case by case for frequency and time-domain problems, which is less obvious for vectorial anisotropic models, as we will see later. Let us give some (non exhaustive) examples of works concerning anisotropic scalar models. In [15], High Orders ABCs have been proposed for the time-dependent anisotropic scalar wave equation and for the convective wave equation. For general time-dependent hyperbolic problems set in an open geometry, standard PMLs are known to give rise to instabilities for some anisotropic models. Indeed this can be explained by the fact that PMLs select outgoing waves according to the phase velocity while the correct selection should be based on the group velocity (see (27) for the exact definitions). For anisotropic models these two velocities differ and this may lead to wrong results as soon as there exist backward waves in the direction of the absorbing layer, i.e. waves for which the projections on the PML direction of the phase and group velocities are of opposite signs [14]. Nevertheless, this difficulty can be overcome for several scalar anisotropic models: stable PMLs have been designed for the anisotropic scalar wave equation [43, 48], aeroacoustics [48], and the linearized Euler equations [71, 65, 72, 84]. Note that backward waves responsible for instabilities may occur also in some dispersive isotropic models, for instance in isotropic elastic waveguides [94, 23]. Concerning time-harmonic problems, one could expect that standard PMLs also fail when they fail in the time-domain, but surprisingly

it is not always the case. In [13] for instance, standard PMLs for the convected wave equation in a waveguide, which are unstable in the time-domain, have been proven to converge in the frequency-domain.

For *vectorial elastic* models, the results are quite different depending on the isotropic or anisotropic nature of the material. For isotropic media, there are still ABCs and PMLs available in the time-harmonic regime ([78] for ABCs, [64] for PMLs) and in the time-domain regime ([51],[68] for ABCs, [40, 11, 52, 75] for PMLs).

For anisotropic elastodynamic models, difficulties arise and there exist much less works. Some time-domain low-order ABCs (which do not always give satisfactory accuracy) have been developed for specific materials [10] and for general anisotropic materials [87, 91], but no high-order accurate ABCs up to our knowledge. Concerning PMLs in time-domain, for a large class of materials which can be specified in terms of the material coefficients [14], standard PMLs are unstable and the question of designing stable PMLs is still open. Some alternative methods have been developed, but they are either (i) not always stable, e.g. the CPMLs, CFS-PMLs and "modal PMLs" which eliminate the long-time instabilities but not the strong instabilities due to backward waves [6, 5, 99, 77] or (ii) no longer perfectly matched, e.g. the SMART method [63, 80, 79], the Double Absorbing Boundary (DAB) [89, 90], Nearly PMLs [41, 38], M-PML [81, 49]. For frequency-domain problems, up to our knowledge there is no literature on PMLs in such media. Our numerical experiments, presented in Section 5.4, will show that PMLs may fail for some materials. Besides, the sensitivity of PMLs to the parameters of the method is even more important for anisotropic models which renders the choice of these parameters more delicate.

Let us now give an overview of existing *non-local* approaches, focusing here on the frequency regime. They are based on the construction of transparent conditions on the artificial boundary, using an exact representation of the solution. Among them, the Boundary Integral Equations (BIE) Methods - which require the knowledge of the Green function that satisfies the radiation condition - are intensively used in various contexts (see for instance [21] for a general presentation).

For elastic wave propagation, in the 80-90's there was a huge literature on "classical Boundary Element Methods" in the harmonic regime (e.g. [74, 92, 3]), most of it concerning isotropic materials. More recently, the emergence and development of methods such as FMM (Fast Multipole Methods) and H-matrices gave new impetus to these BIE methods. We only cite some of these recent works for time-harmonic elastic waves [31] and the references herein, [35, 36, 42] for the Fast Multipole Method (FMM) in the full space, [34] for FM-BEM (Fast Multipole Boundary Element Methods) in semi-infinite media, [37] for H-matrices. Let us emphasize that while for isotropic elastic waves, the Green function is known explicitly, this is not true anymore for anisotropic media. Its computation via for instance Fourier transforms is costly, especially since it does not only depend on the distance between two points but also on their orientation, contrary to the isotropic case.

When a separation of variables is available, one can also derive a modal expression of the DtN operator

on an appropriate artificial boundary. This has been done for the isotropic and anisotropic scalar cases [58], and for the isotropic elastic case [73]. But such approach cannot be extended to anisotropic elastic media to our knowledge.

Since there are no satisfying methods for dealing with time-harmonic elastic waves in anisotropic unbounded media, a new method, the so-called Half-Space Matching (HSM) method, has been designed, inspired by the works developped in [53, 54] . This method has been first presented on a scalar model [46, 26, 45, 95], more precisely in the context of time-harmonic acoustic wave propagation in a 2D medium which is a local perturbation of an unbounded isotropic or anisotropic homogeneous medium. The idea is to take advantage of the homogeneity of the medium outside the perturbation, hence in particular in half-planes (typically four in 2D) surrounding the defect, which allows to write an explicit integral expression of the solution with respect to its trace on the artificial boundary delimiting the considered half-plane. This finally gives a system whose unknowns are the restriction of the solution in a bounded domain around the perturbation and the four traces of the solution on the four artificial boundaries. The equations ensure the compatibility of the representations in the overlapping zones where at least two different representations coexist. This coupled system can be discretized by Finite Elements, 1D for the trace unknowns, and 2D for the volume unknown.

Furthermore, the computation of the traces enables to reconstruct a posteriori the solution in the half-planes (and therefore in the whole domain), which is impossible for instance when using non exact absorbing boundary conditions or PML. Another advantage of this method, as for other non-local methods, is to naturally take into account evanescent waves which is rarely the case with local methods, except in some specific works [5, 61].

The purpose of the present paper is to extend this work to the 2D vectorial elastic model, considering isotropic and anisotropic materials.

We first introduce the problem in Section 2. In Section 3, we recall the classical plane wave analysis in the context of general anisotropic models. The principles of the HSM method are presented in Section 4.1. The method relies on the expression of half-space solutions which are given for isotropic materials in Section 4.2 and for anisotropic materials in Section 4.3. Section 5 is devoted to the numerical aspects of the method. Subsection 5.1 presents the discretization scheme. Then, the method is validated, in Section 5.2 in the isotropic case and in Section 5.3 in the anisotropic case. In Section 5.4, a comparison with PMLs shows that, unlike the HSM method, PMLs are very sensitive to the choice of parameters, especially for anisotropic materials.

2. Problem setting

We consider in this paper the two-dimensional linear elastic wave scattering problem by a bounded obstacle $\mathcal{O} \subset \mathbb{R}^2$ in a frequency-domain regime. The following equations are deduced from the elastodynamic equations assuming a time-dependency $e^{-\mathrm{i}\omega t}$ at a given frequency $\omega > 0$:

$$\left| \begin{array}{ll} -\mathrm{div}\,\sigma(\mathbf{u}) - \widetilde{\rho}\,\omega^2 \mathbf{u} = \mathbf{f} & \text{in } \Omega = \mathbb{R}^2 \setminus \mathcal{O}, \\ \sigma(\mathbf{u})\nu = \mathbf{g} & \text{on } \partial\mathcal{O} \end{array} \right. \tag{1}$$

where $\widetilde{\rho} = \widetilde{\rho}(x, y)$ is the mass density of the material and ν is the unit normal on $\partial\mathcal{O}$, oriented towards the exterior of Ω (or equivalently towards the interior of $\mathcal{O}$). We suppose that $\widetilde{\rho}$ takes a constant value ρ outside a bounded domain (see (7)). More generally, the medium (whose material coefficients are denoted with $\widetilde{\cdot}$) is supposed to be a local perturbation of a homogeneous background (whose material coefficients are denoted without $\widetilde{\cdot}$). The small strains assumption implies that the stress tensor σ is linked to the displacement field $\mathbf{u}$ by the general Hooke's law [93, 33]

$$\sigma(\mathbf{u}) := \begin{bmatrix} \sigma_{xx}(\mathbf{u}) & \sigma_{xy}(\mathbf{u}) \\ \sigma_{xy}(\mathbf{u}) & \sigma_{yy}(\mathbf{u}) \end{bmatrix} = \widetilde{\mathbf{C}}\varepsilon(\mathbf{u}) \tag{2}$$

where $\varepsilon(\mathbf{u})$ is the strain tensor

$$\varepsilon(\mathbf{u}) = \begin{bmatrix} \varepsilon_{xx}(\mathbf{u}) & \varepsilon_{xy}(\mathbf{u}) \\ \varepsilon_{xy}(\mathbf{u}) & \varepsilon_{yy}(\mathbf{u}) \end{bmatrix}, \quad \varepsilon_{ij}(\mathbf{u}) = \frac{1}{2}(\partial_i \mathbf{u}_j + \partial_j \mathbf{u}_i), \quad i, j \in \{x, y\}, \tag{3}$$

and $\widetilde{\mathbf{C}} = \widetilde{\mathbf{C}}(x, y)$ is the fourth-order rigidity tensor satisfying the classical symmetries

$$\widetilde{\mathbf{C}}_{ijkl} = \widetilde{\mathbf{C}}_{klij} = \widetilde{\mathbf{C}}_{ijlk}, \quad \forall i, j, k, l \in \{x, y\}.$$

Moreover, $\widetilde{\mathbf{C}}$ is positive definite, *i.e.* there exists $\alpha > 0$ such that, for all symmetric second-order tensors $\xi \in \mathbb{C}^{2\times 2}$, one has (with the Einstein convention):

$$\forall (x, y) \in \Omega, \;\; \widetilde{\mathbf{C}}(x, y)\xi : \overline{\xi} := \widetilde{\mathbf{C}}_{ijkl}(x, y)\xi_{ij}\overline{\xi}_{kl} \geq \alpha|\xi|^2 = \alpha\xi_{ij}\overline{\xi}_{ij}. \tag{4}$$

Using the Voigt notation [33], this fourth-order tensor can be represented by a 3×3 symmetric matrix denoted by $\widetilde{C} = \widetilde{C}(x, y)$ such that Hooke's law is equivalent to :

$$\begin{bmatrix} \sigma_{xx}(\mathbf{u}) \\ \sigma_{yy}(\mathbf{u}) \\ \sigma_{xy}(\mathbf{u}) \end{bmatrix} = \begin{bmatrix} \widetilde{C}_{11} & \widetilde{C}_{12} & \widetilde{C}_{13} \\ \widetilde{C}_{12} & \widetilde{C}_{22} & \widetilde{C}_{23} \\ \widetilde{C}_{13} & \widetilde{C}_{23} & \widetilde{C}_{33} \end{bmatrix} \begin{bmatrix} \varepsilon_{xx}(\mathbf{u}) \\ \varepsilon_{yy}(\mathbf{u}) \\ 2\varepsilon_{xy}(\mathbf{u}) \end{bmatrix}. \tag{5}$$

For any symmetric second-order tensor $\xi \in \mathbb{C}^{2\times 2}$, if we introduce a corresponding vector $V(\xi) \in \mathbb{C}^3$:

$$V(\xi) = (\xi_{xx}, \xi_{yy}, 2\xi_{xy})^t,$$

one has

$$\widetilde{\mathbf{C}}\xi : \overline{\xi} = \widetilde{C}(x,y)V(\xi)\cdot\overline{V(\xi)}.$$

The property (4) is then equivalent to the positive definite character of the matrix $\widetilde{C}$:

$$\forall (x,y)\in\Omega,\ \ \widetilde{C}(x,y)V\cdot\overline{V}\geq\alpha|V|^2,\quad \forall V\in\mathbb{C}^3. \tag{6}$$

In the sequel, we suppose that there exists a constant $a>0$ such that

$$\mathcal{O}\cup\mathrm{Supp}(\mathbf{f})\cup\mathrm{Supp}(\widetilde{\rho}-\rho)\cup\mathrm{Supp}(\widetilde{C}-C)\subset(-a,a)^2, \tag{7}$$

where ρ and C are constant parameters characterizing the background material and we set

$$\Omega_a := (-a,a)^2\setminus\mathcal{O}. \tag{8}$$

As usual, we say that the background is

- isotropic if

$$C_{13}=C_{23}=0,\ C_{11}=C_{22}=\lambda+2\mu,\ C_{12}=\lambda,\ C_{33}=\mu, \tag{9}$$

  where λ and μ are the well-known Lamé coefficients,

- orthotropic if

$$C_{13}=C_{23}=0,$$

- general anisotropic if $C_{13}\neq 0$ and/or $C_{23}\neq 0$.

As mentioned in the introduction, the case of isotropic backgrounds (C satisfying (9)) is widely studied in the literature whereas general backgrounds still raise theoretical and numerical questions.

The equations (1) have to be completed by a condition at infinity to select the "outgoing" or the "radiating" solution. For isotropic backgrounds (C satisfying (9)), this can be achieved through the *Kupradze-Sommerfeld radiation condition*, which writes as folllows

$$\left(\partial_{|\mathbf{x}|}-i\frac{\omega}{c_P}\right)\mathrm{div}\,\mathbf{u}=\mathrm{o}(|\mathbf{x}|^{-\frac{1}{2}})\quad\text{and}\quad\left(\partial_{|\mathbf{x}|}-i\frac{\omega}{c_S}\right)\mathrm{rot}\,\mathbf{u}=\mathbf{o}(|\mathbf{x}|^{-\frac{1}{2}}),\ \ |\mathbf{x}|\to+\infty \tag{10}$$

where

$$c_P^2=(\lambda+2\mu)/\rho\quad\text{and}\quad c_S^2=\mu/\rho. \tag{11}$$

As proven in [29], the problem (1-10) is well-posed in the classical mathematical framework. In particular, if $\mathbf{f}\in[L^2(\Omega_a)]^2$ and $\mathbf{g}\in L^2(\partial\mathcal{O})^2$, the solution $\mathbf{u}$ belongs to $[H^1_{loc}(\Omega)]^2$, which means that for all $R>0$,

$$\int_{\Omega\cap\{|\mathbf{x}|<R\}}|\mathbf{u}|^2+|\nabla u_x|^2+|\nabla u_y|^2<+\infty.$$

For anisotropic materials, a radiation condition similar to (10) is not known up to our knowledge. Let us mention [22] which proposed a well-posed volume integral equation formulation based on the Green's function of the anisotropic background. In this work, we propose another definition of the outgoing solution of (1) which is coherent with (10) for isotropic materials. More precisely, the solution has to be outgoing in four half-spaces covering the whole domain at infinity (see Section 4.2 for isotropic background and Section 4.3 for anisotropic background).

3. Plane waves and slowness curves

The plane wave analysis, also known as Kelvin Christoffel analysis (see for instance [33, Section 1.3] for 3D problems) is the main tool for understanding wave phenomena in homogeneous anisotropic media. A well-known and important feature of anisotropic media is that group and phase velocities of plane waves may differ, contrary to isotropic media. This plays a key role in the description of outgoing waves. In the present paper, outgoing plane waves appear in the half-space representations that are derived in Sections 4.2 and 4.3. Plane waves are also used for analyzing PML methods for some anisotropic models (see Section 5.4).

We consider the time-harmonic elastodynamic equation

$$-\mathrm{div}\,\sigma(\mathbf{u}) - \rho\omega^2\mathbf{u} = 0 \quad \text{in } \mathbb{R}^2, \tag{12}$$

in a homogeneous material. We look for plane wave solutions of (12) of the form

$$\mathbf{u} = \mathbf{U}e^{\mathrm{i}(k_x x + k_y y)}, \quad \mathbf{U} \in \mathbb{C}^2 \setminus \{0\}, \tag{13}$$

where $\mathbf{k} := (k_x, k_y) \in \mathbb{R}^2$ is the wave vector and $\mathbf{U}$ the polarization vector. From (5), one deduces that

$$\begin{bmatrix} \sigma_{xx}(\mathbf{u}) \\ \sigma_{xy}(\mathbf{u}) \end{bmatrix} = (ik_x\mathcal{A}_0 + ik_y\mathcal{A}_1)\,\mathbf{u} \quad \text{and} \quad \begin{bmatrix} \sigma_{xy}(\mathbf{u}) \\ \sigma_{yy}(\mathbf{u}) \end{bmatrix} = \left(ik_x\mathcal{A}_1^{\mathrm{T}} + ik_y\mathcal{A}_2\right)\mathbf{u} \tag{14}$$

where

$$\mathcal{A}_0 = \begin{bmatrix} C_{11} & C_{13} \\ C_{13} & C_{33} \end{bmatrix}, \quad \mathcal{A}_1 = \begin{bmatrix} C_{13} & C_{12} \\ C_{33} & C_{23} \end{bmatrix}, \quad \mathcal{A}_2 = \begin{bmatrix} C_{33} & C_{23} \\ C_{23} & C_{22} \end{bmatrix}, \tag{15}$$

and $\mathcal{A}_1^{\mathrm{T}}$ denotes the transpose of the matrix $\mathcal{A}_1$. Noting that

$$\mathrm{div}\,\sigma(\mathbf{u}) = ik_x \begin{bmatrix} \sigma_{xx}(\mathbf{u}) \\ \sigma_{xy}(\mathbf{u}) \end{bmatrix} + ik_y \begin{bmatrix} \sigma_{xy}(\mathbf{u}) \\ \sigma_{yy}(\mathbf{u}) \end{bmatrix},$$

one can check that a vector field $\mathbf{u}$ of the form (13) is a solution of (12) if and only if

$$\mathcal{A}(\mathbf{k})\mathbf{U} = \omega^2\mathbf{U}$$

where

$$\mathcal{A}(\mathbf{k}) = \frac{1}{\rho}\left[k_x^2\mathcal{A}_0 + k_xk_y(\mathcal{A}_1 + \mathcal{A}_1^{\mathrm{T}}) + k_y^2\mathcal{A}_2\right]. \tag{16}$$

This leads to the following so-called dispersion relation of plane waves which links ω and $\mathbf{k}$:

$$\mathcal{F}(\mathbf{k},\omega) = 0 \quad \text{with} \quad \mathcal{F}(\mathbf{k},\omega) = \det(\mathcal{A}(\mathbf{k}) - \omega^2\mathcal{I}_2). \tag{17}$$

Since the dependency in ω of $\mathcal{F}(\mathbf{k},\omega)$ is only in ω^2, one can assume without loss of generality that $\omega > 0$. Note that $\mathcal{F}(\mathbf{k},\omega)$ is a homogeneous polynomial in k_x, k_y and ω of degree 4, i.e. $\mathcal{F}(\lambda\mathbf{k},\lambda\omega) = \lambda^4\mathcal{F}(\mathbf{k},\omega)$. Therefore it satisfies the Euler identity

$$\mathbf{k}\cdot\nabla_{\mathbf{k}}\mathcal{F}(\mathbf{k},\omega) + \omega\frac{\partial\mathcal{F}}{\partial\omega}(\mathbf{k},\omega) = 4\mathcal{F}(\mathbf{k},\omega). \tag{18}$$

One can deduce the following implication which will be useful later on :

$$\mathcal{F}(k_x,k_y,\omega) = 0 \Longrightarrow \mathbf{k}\cdot\nabla_{\mathbf{k}}\mathcal{F}(\mathbf{k},\omega) + \omega\frac{\partial\mathcal{F}}{\partial\omega}(\mathbf{k},\omega) = 0 \tag{19}$$

From the definition of $\mathcal{A}(\mathbf{k})$, it is easy to see that for all materials

$$\mathcal{F}(\mathbf{k},\omega) = 0 \quad \Leftrightarrow \quad \mathcal{F}(-k_x,-k_y,\omega) = 0. \tag{20}$$

Additional symmetries occur for orthotropic materials. Indeed, if $C_{13} = C_{23} = 0$,

$$\mathcal{F}(k_x,k_y,\omega) = 0 \quad \Leftrightarrow \quad \mathcal{F}(k_x,-k_y,\omega) = 0 \quad \Leftrightarrow \quad \mathcal{F}(-k_x,k_y,\omega) = 0. \tag{21}$$

Finally, for isotropic materials, the dispersion relation simplifies and gives rise to two uncoupled dispersion relations:

$$\mathcal{F}(k_x,k_y,\omega) = 0 \quad \Leftrightarrow \quad k_x^2 + k_y^2 = k_P^2 \quad \text{or} \quad k_x^2 + k_y^2 = k_S^2 \tag{22}$$

where

$$k_P = \frac{\omega}{c_P} \quad \text{and} \quad k_S = \frac{\omega}{c_S} \tag{23}$$

and c_P and c_S are defined as in (11).

By homogeneity we have for all $\omega > 0$

$$\mathcal{F}(k_x,k_y,\omega) = \omega^4\,\mathcal{F}\left(\frac{k_x}{\omega},\frac{k_y}{\omega},1\right). \tag{24}$$

This leads to define the so-called *slowness diagram*

$$\mathcal{S} \;=\; \{(\xi_x,\xi_y)\in\mathbb{R}^2 \quad \text{where} \quad \mathcal{F}(\xi_x,\xi_y,1) = 0\}. \tag{25}$$

By definition, a plane wave $\mathbf{u} = \mathbf{U}e^{\mathrm{i}(k_xx+k_yy)}$ is such that $(k_x/\omega, k_y/\omega)\in\mathcal{S}$. Writing $s_y = \alpha s_x$ with $\alpha\in\mathbb{R}$, one can check that $(s_x,\alpha s_x)\in\mathcal{S}$ if and only if $s_x = \pm 1/\sqrt{\lambda_1(\alpha)}$ or $s_x = \pm 1/\sqrt{\lambda_2(\alpha)}$ where $\lambda_1(\alpha)$ and $\lambda_2(\alpha)$

are the two positive eigenvalues of the symmetric definite positive matrix $\mathcal{A}(1,\alpha)$. These two eigenvalues continuously depend on α and are distinct except maybe at a finite set of values of α (including eventually $\alpha = \pm\infty$ for $s_x = 0$). As a consequence the slowness diagram is composed of two distinct closed and star-shaped curves, called the *slowness curves*. Figure 1 shows slowness curves (for a density $\rho = 1$) associated to various materials whose characteristics are :

$$\begin{aligned} &\textbf{(ISO)} \quad C = \begin{bmatrix} 20 & 16 & 0 \\ 16 & 20 & 0 \\ 0 & 0 & 2 \end{bmatrix}, \qquad \textbf{(O1)} \quad C = \begin{bmatrix} 20 & 3.8 & 0 \\ 3.8 & 20 & 0 \\ 0 & 0 & 2 \end{bmatrix}, \\ &\textbf{(O2)} \quad C = \begin{bmatrix} 4 & 7.5 & 0 \\ 7.5 & 20 & 0 \\ 0 & 0 & 2 \end{bmatrix}, \qquad \textbf{(A)} \quad C = \begin{bmatrix} 6 & 8 & 2 \\ 8 & 21 & 10 \\ 2 & 10 & 30 \end{bmatrix}. \end{aligned} \tag{26}$$

The first material is isotropic ($\lambda = 16$, $\mu = 2$), the second and the third materials are taken from [14] and are orthotropic materials, whereas the last one is a general anisotropic medium.

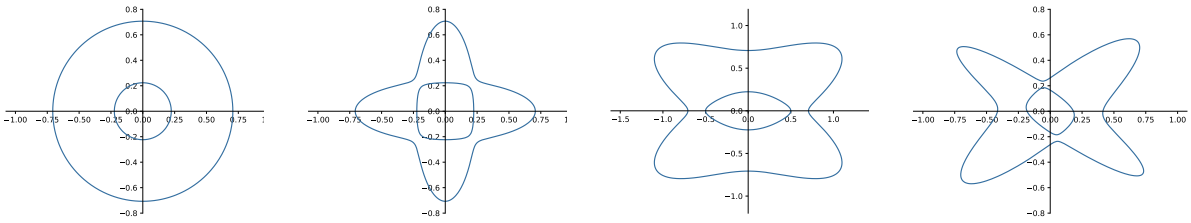

(ISO) **(O1)** **(O2)** **(A)**

Figure 1: Slowness diagrams of the materials whose characteristics are given in (26).

The slowness curves for an isotropic material are two circles which illustrates (22). In general, the slowness curves are not circles anymore but they have some symmetries, which illustrates (20) for general materials and (21) for orthotropic materials.

A crucial point for our purpose is to know the direction of propagation of plane waves. More specifically, the derivation of the half-space representation requires to discriminate plane waves according to their direction of propagation along directions x or y (and this is also used to explain instabilities of cartesian PMLs in anisotropic media [14]). We explain below how this discrimination can be done, and how it is related graphically to the above slowness diagrams.

In anisotropic media, it is well-known that the physical relevant direction of propagation is given by the group velocity $\mathbf{v}_g$, which is the energy velocity, and not by the phase velocity $\mathbf{v}_p$.

To define the phase velocity and the group velocity at a point of a slowness curve, we fix $\mathbf{k}$ and we consider (17) as an equation in ω. Note that for all $\mathbf{k}$, $\mathcal{F}(\mathbf{k},\cdot)$ is a polynomial of order 2 in ω^2 and by the hyperbolicity of the equation, there are four real roots, that we denote $\pm\omega_1(\mathbf{k}), \pm\omega_2(\mathbf{k})$ where $\omega_j(\mathbf{k}) > 0, j = 1, 2$. These roots $\omega_j(\mathbf{k}), j = 1, 2$ are differentiable (even analytic) with respect to $\mathbf{k}$ except for at most a finite set of $\mathbf{k}$ for which $\omega_1(\mathbf{k}) = \omega_2(\mathbf{k})$. Except for these values, one can check that $\partial_\omega \mathcal{F}(\mathbf{k}, \omega_j(\mathbf{k})) \neq 0$ for $j = 1, 2$. The phase velocity $\mathbf{v}_p(\mathbf{k})$ and the group velocity $\mathbf{v}_g(\mathbf{k})$ (defined except at most for a finite set of $\mathbf{k}$) of the associated plane waves $\mathbf{u}(x, y) = \mathbf{U}e^{i(k_x x + k_y y)}$ are then given by (see e.g. [14])

$$\mathbf{v}_p(\mathbf{k}) = \frac{\omega(\mathbf{k})}{|\mathbf{k}|}\frac{\mathbf{k}}{|\mathbf{k}|}, \quad \mathbf{v}_g(\mathbf{k}) = \nabla_{\mathbf{k}}\omega(\mathbf{k}), \quad \mathbf{k} = (k_x, k_y). \tag{27}$$

with $\omega(\mathbf{k}) = \omega_1(\mathbf{k})$ or $\omega_2(\mathbf{k})$.

The plane wave propagates towards $x \to +\infty$ if $\mathbf{v}_g(k_x, k_y)\cdot\mathbf{e}_x > 0$ and towards $x \to -\infty$ if $\mathbf{v}_g(k_x, k_y)\cdot\mathbf{e}_x < 0$. To explain how this sign can be obtained graphically thanks to the slowness curves, let us now express the group velocity in terms of the function $\mathcal{F}$. If we differentiate (17) with respect to $\mathbf{k}$, we obtain

$$\nabla_{\mathbf{k}}\mathcal{F}(\mathbf{k}, \omega(\mathbf{k})) + \frac{\partial \mathcal{F}}{\partial \omega}(\mathbf{k}, \omega(\mathbf{k}))\mathbf{v}_g(\mathbf{k}) = 0. \tag{28}$$

Using (19), we finally obtain

$$\mathbf{v}_g(\mathbf{k}) = \frac{\omega \nabla_{\mathbf{k}}\mathcal{F}(\mathbf{k}, \omega(\mathbf{k}))}{\mathbf{k}\cdot\nabla_{\mathbf{k}}\mathcal{F}(\mathbf{k}, \omega(\mathbf{k}))}$$

and consequently $\mathbf{k}\cdot\mathbf{v}_g(\mathbf{k}) = \omega(\mathbf{k})$. This shows that $\mathbf{v}_g(\mathbf{k})$ is colinear to the outward normal to the slowness curve at $(\xi_1, \xi_2) = (k_x/\omega, k_y/\omega)$ and oriented in the same direction. In conclusion, to know if the plane wave $\mathbf{u}(x, y) = \mathbf{U}e^{i(k_x x + k_y y)}$ propagates towards $x \to +\infty$ (resp. $x \to -\infty$), one can look at the outward normal to the slowness curve at $(\xi_1, \xi_2) = (k_x/\omega, k_y/\omega)$ and check if it points towards $x \to +\infty$ (resp. $x \to -\infty$). In the isotropic case, the slowness curves being simple circles, the plane wave propagates towards $x \to +\infty$ (resp. $x \to -\infty$) if $k_x > 0$ (resp. $k_x < 0$). In other words, for the isotropic case, it suffices to look at the phase velocity. However, this is not the case in general, see Figure 2.

This graphical characterization of the outgoing wave is not directly used for the derivation of the half-space representation. We use instead the energy flux of a plane wave $\mathbf{u}$ in the direction $\mathbf{e}_x$ defined by

$$\Im(\sigma(\mathbf{u})\mathbf{e}_x \cdot \bar{\mathbf{u}}).$$

Note that this quantity is independent of x and y. Indeed by (14),

$$\Im(\sigma(\mathbf{u})\mathbf{e}_x \cdot \bar{\mathbf{u}}) = k_x \overline{\mathbf{U}}^{\mathrm{T}}\mathcal{A}_0\mathbf{U} + k_y \Re\left(\overline{\mathbf{U}}^{\mathrm{T}}\mathcal{A}_1\mathbf{U}\right) = k_x \overline{\mathbf{U}}^{\mathrm{T}}\mathcal{A}_0\mathbf{U} + \frac{k_y}{2}\overline{\mathbf{U}}^{\mathrm{T}}(\mathcal{A}_1 + \mathcal{A}_1^{\mathrm{T}})\mathbf{U}. \tag{29}$$

It is known (and proven in appendix A) that

$$[\Im(\sigma(\mathbf{u})\mathbf{e}_x \cdot \bar{\mathbf{u}})]\,[\mathbf{v}_g(k_x, k_y)\cdot\mathbf{e}_x] > 0, \tag{30}$$

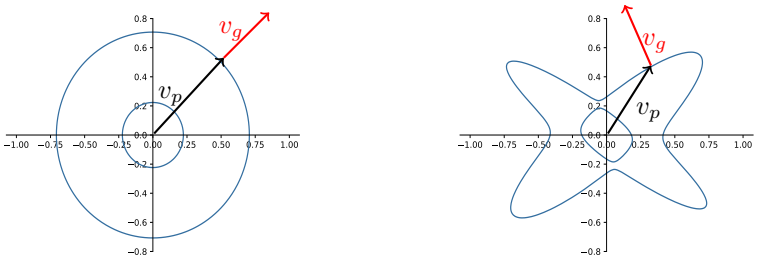

(ISO) **(A)**

Figure 2: Phase velocity (black arrow) and group velocity (red arrow) on the slowness diagram of an isotropic medium (left) and of an anisotropic medium (right).

so that a plane wave $\mathbf{u}(x,y) = \mathbf{U}e^{i(k_x x + k_y y)}$ propagates towards $x \to +\infty$ (resp. $x \to -\infty$) if and only if $\Im(\sigma(\mathbf{u})\mathbf{e}_x \cdot \bar{\mathbf{u}}) > 0$ (resp. $\Im(\sigma(\mathbf{u})\mathbf{e}_x \cdot \bar{\mathbf{u}}) < 0$). Similarly, $\mathbf{u}(x,y) = \mathbf{U}e^{i(k_x x + k_y y)}$ propagates towards $y \to +\infty$ (resp. $y \to -\infty$) if and only if $\Im(\sigma(\mathbf{u})\mathbf{e}_y \cdot \bar{\mathbf{u}}) > 0$ (resp. $\Im(\sigma(\mathbf{u})\mathbf{e}_y \cdot \bar{\mathbf{u}}) < 0$) where

$$\Im(\sigma(\mathbf{u})\mathbf{e}_y \cdot \bar{\mathbf{u}}) = k_y \overline{\mathbf{U}}^{\mathrm{T}} \mathcal{A}_2 \mathbf{U} + \frac{k_x}{2} \overline{\mathbf{U}}^{\mathrm{T}} (\mathcal{A}_1 + \mathcal{A}_1^{\mathrm{T}}) \mathbf{U}$$

4. The Half-Space Matching (HSM) Method

4.1. Abstract formulation

Let us now consider Problem (1). In this section, we explain how to reformulate this problem with the Half-Space Matching method, as described in [96, 46] for the case of scalar equations. The main idea is to couple several representations of the solution in five subdomains which overlap (see Figure 3). Let us recall that the parameter $a > 0$ and the interior domain Ω_a are defined in (7)-(8). We also introduce:

- a larger domain $\Omega_b = (-b,b)^2 \setminus \mathcal{O}$ with $b > a$,
- four half-spaces $\Omega^j = \{x_j > a\} \times \{y_j \in \mathbb{R}\}$ (whose boundaries will be denoted Σ^j), where the local coordinates (x_j, y_j) are defined by

$$\begin{bmatrix} x_j \\ y_j \end{bmatrix} = \mathcal{R}(\theta_j) \begin{bmatrix} x \\ y \end{bmatrix} \quad \text{with } \mathcal{R}(\theta_j) = \begin{bmatrix} \cos(\theta_j) & \sin(\theta_j) \\ -\sin(\theta_j) & \cos(\theta_j) \end{bmatrix} \text{ and } \theta_j = \frac{j\pi}{2}, \quad j \in [\![0,3]\!] := \{0,1,2,3\}. \tag{31}$$

The boundary of Ω_b is split into four parts $\Sigma_{bb}^j = \{x_j = b\} \times \{y_j \in (-b,b)\}$, $j \in [\![0,3]\!]$. Similarly, we will denote $\Sigma_{aa}^j = \{x_j = a\} \times \{y_j \in (-a,a)\}$, $j \in [\![0,3]\!]$ the four segments of the exterior boundary of Ω_a.

We denote by $\mathbf{u}^b$ (resp. $\mathbf{u}^j$) the restriction of the solution $\mathbf{u}$ in Ω_b (resp. Ω^j). As the subdomains overlap and since $\mathbf{u}^b$ and $\mathbf{u}^j$ all represent the same function, we have

$$\mathbf{u}^b = \mathbf{u}^j \ \text{ in } \ \Omega_b \cap \Omega^j, \quad j \in [\![0,3]\!] \tag{32}$$

and

$$\mathbf{u}^j = \mathbf{u}^{j+1} \ \text{ in } \ \Omega^j \cap \Omega^{j+1}, \quad j \in [\![0,3]\!], \tag{33}$$

where we have set $\mathbf{u}^4 = \mathbf{u}^0$ and $\Omega^4 = \Omega^0$, which amounts to identify $[\![0,3]\!]$ to $\mathbb{Z}/4\mathbb{Z}$. It will be convenient to make this identification systematically in the sequel. The compatibility relations (32) and (33), which are obvious for now, are the key properties to derive the HSM formulation. First, by definition, $\mathbf{u}^b$ satisfies the following equations:

$$\left| \begin{array}{lll} -\mathrm{div}\,\sigma(\mathbf{u}^b) - \widetilde{\rho}\,\omega^2 \mathbf{u}^b = \mathbf{f} & \text{in} & \Omega_b, \\ \sigma(\mathbf{u}^b)\nu = \mathbf{g} & \text{on} & \partial\mathcal{O}, \end{array} \right. \tag{34}$$

and similarly $\mathbf{u}^j$ satisfies:

$$\left| -\mathrm{div}\,\sigma(\mathbf{u}^j) - \rho\,\omega^2 \mathbf{u}^j = 0 \quad \text{in} \quad \Omega^j, \quad j \in [\![0,3]\!]. \right. \tag{35}$$

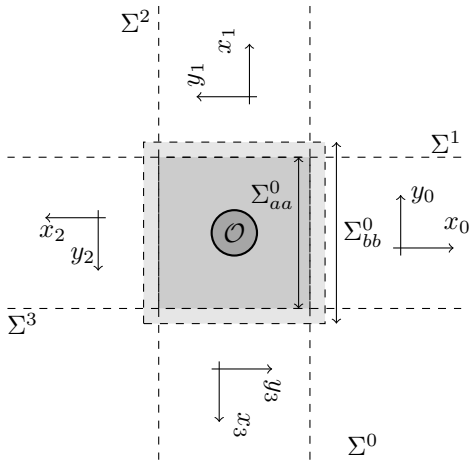

Figure 3: Notations : the domain Ω_b is the largest square represented in light gray and the domain Ω_a is the interior square in stronger grey. The obstacle $\mathcal{O}$ is represented by the small circle in the strongest gray.

An important remark is that the outgoing solution $\mathbf{u}^j$ of (35) in each half-space Ω^j can be expressed in terms of its trace $\mathbf{\Phi}^j$ on the boundary Σ^j by using a Fourier transform in the direction of the boundary. The construction of such integral representation, which corresponds to a superposition of outgoing plane waves (see Section 3) and evanescent waves, is detailed in Section 4.2 for isotropic materials and Section 4.3 for anisotropic materials. For now, we will write

$$\mathbf{u}^j = \mathbf{U}^j(\mathbf{\Phi}^j) \quad \text{in } \Omega^j, \quad j \in [\![0,3]\!], \tag{36}$$

where $\mathbf{U}^j(\mathbf{\Phi})$ is called a half-space solution and is the outgoing solution of (35) in Ω^j with the given trace $\mathbf{\Phi}$ on Σ^j:

$$\left| \begin{array}{lll} -\mathrm{div}\,\sigma(\mathbf{U}^j(\mathbf{\Phi})) - \rho\omega^2\mathbf{U}^j(\mathbf{\Phi}) = 0 & \text{in} & \Omega^j, \\ \\ \mathbf{U}^j(\mathbf{\Phi}) = \mathbf{\Phi} & \text{on} & \Sigma^j. \end{array} \right. , \quad j \in [\![0,3]\!], \tag{37}$$

The idea of the method is to reformulate the problem in terms of $\mathbf{u}^b$, a "volume" unknown, (which corresponds to the solution in Ω_b) and $\mathbf{\Phi}^j$, $j \in [\![0,3]\!]$, the "surface" unknowns (which correspond to the traces of the solution on the Σ^j's).

To construct the system of equations linking these unknowns, we use first the compatibility relations (32) which implies, in terms of the new unknowns

$$\left| \begin{array}{lll} \mathbf{u}^b = \mathbf{\Phi}^j & \text{on} & \Sigma^j_{aa}, \\ \\ \sigma(\mathbf{u}^b)\nu^j = \sigma(\mathbf{U}^j(\mathbf{\Phi}^j))\nu^j & \text{on} & \Sigma^j_{bb}, \end{array} \right. , \quad j \in [\![0,3]\!], \tag{38}$$

where ν^j is the unit normal vector to Σ^j_{bb} pointing towards the exterior of Ω_b. In the spirit of Domain Decomposition Methods [44], the compatibility conditions on the Neumann traces can be substituted by a condition on Robin-like traces as follows

$$\left| \begin{array}{lll} \mathbf{u}^b = \mathbf{\Phi}^j & \text{on} & \Sigma^j_{aa}, \\ \\ \sigma(\mathbf{u}^b)\nu^j - i\gamma^j\mathbf{u}^b = \Lambda^j(\mathbf{\Phi}^j) & \text{on} & \Sigma^j_{bb}, \end{array} \right. , \quad j \in [\![0,3]\!], \tag{39}$$

where for all j, γ^j is a symmetric positive definite matrix and the operator Λ^j relates the trace $\mathbf{\Phi}$ on Σ^j to the Robin data on Σ^j_{bb}

$$\forall \mathbf{\Phi}, \quad \Lambda^j(\mathbf{\Phi}) = \left[\sigma(\mathbf{U}^j(\mathbf{\Phi}))\nu^j - i\gamma^j\mathbf{U}^j(\mathbf{\Phi})\right]|_{\Sigma^j_{bb}}, \quad j \in [\![0,3]\!]. \tag{40}$$

Note that if $\gamma^j = 0$, (39) is nothing else but (38), and Λ^j is simply the so-called Dirichlet-to-Neumann (DtN) operator. We will see later on the advantages of introducing $\gamma^j \neq 0$. In principle, γ^j can be any symmetric positive definite matrix. A particular choice will be motivated in Section 5.1. The Fourier integral representation of these Dirichlet-to-Robin (DtR) operators are given in Section 4.2 for isotropic materials and Section 4.3 for anisotropic materials.

These equations have to be completed by equations linking the $\mathbf{\Phi}^j$'s on the infinite half-lines $\Sigma^{j\pm1} \cap \Omega^j$. We use for that the compatibility relations (33). By writing that for all j, $\mathbf{u}^j = \mathbf{U}^j(\mathbf{\Phi}^j)$ and $\mathbf{u}^{j+1} = \mathbf{U}^{j+1}(\mathbf{\Phi}^{j+1})$ have to coincide on $\Sigma^j \cap \Omega^{j+1}$ and $\Sigma^{j+1} \cap \Omega^j$, we obtain that

$$\mathbf{\Phi}^j = \mathbf{U}^{j+1}(\mathbf{\Phi}^{j+1}) \quad \text{on } \Sigma^j \cap \Omega^{j+1} \quad \text{and} \quad \mathbf{\Phi}^{j+1} = \mathbf{U}^j(\mathbf{\Phi}^j) \quad \text{on } \Sigma^{j+1} \cap \Omega^j, \quad j \in [\![0,3]\!]. \tag{41}$$

By introducing the Dirichlet-to-Dirichlet (DtD) type operators $D^j_{j\pm1}$ defined by

$$\forall \mathbf{\Phi}, \quad D^j_{j\pm1}\,\mathbf{\Phi} := \mathbf{U}^j(\mathbf{\Phi})\Big|_{\Sigma^{j\pm1}\cap\Omega^j}, \quad j\in[\![0,3]\!], \tag{42}$$

the relations (41) rewrite for all j

$$\mathbf{\Phi}^j = D^{j+1}_j\,\mathbf{\Phi}^{j+1} \quad \text{on } \Sigma^j\cap\Omega^{j+1} \quad \text{and} \quad \mathbf{\Phi}^{j+1} = D^j_{j+1}\,\mathbf{\Phi}^j \quad \text{on } \Sigma^{j+1}\cap\Omega^j, \quad j\in[\![0,3]\!]. \tag{43}$$

The Fourier integral representations of these DtD operators are given in Section 4.2 for isotropic materials and Section 4.3 for anisotropic materials.

To sum up, the HSM formulation is given by gathering relations (34), (39) and (43):

$$\left|\begin{array}{lll} -\mathrm{div}\,\sigma(\mathbf{u}^b) - \rho\omega^2\mathbf{u}^b = \mathbf{f} & \text{in} & \Omega_b \\ \sigma(\mathbf{u}^b)\nu = \mathbf{g} & \text{on} & \partial\mathcal{O} \\ \sigma(\mathbf{u}^b)\nu^j - i\gamma^j\mathbf{u}^b = \Lambda^j\mathbf{\Phi}^j & \text{on} & \Sigma^j_{bb}, \quad j\in[\![0,3]\!] \\ \mathbf{\Phi}^j = \mathbf{u}^b & \text{on} & \Sigma^j_{aa}, \quad j\in[\![0,3]\!] \\ \mathbf{\Phi}^{j\pm1} = D^j_{j\pm1}\mathbf{\Phi}^j & \text{on} & \Sigma^{j\pm1}\cap\Omega^j, \quad j\in[\![0,3]\!] \end{array}\right. \tag{44}$$

Remark 4.1. *Note that it is natural to express the trace $\mathbf{\Phi}^j$, the half-space solution $\mathbf{U}^j(\mathbf{\Phi}^j)$ and then $D^j_{j\pm1}\mathbf{\Phi}^j$, in the coordinates (x_j,y_j). A technical difficulty is that for instance, in the first equality of (43), $\mathbf{\Phi}^j$ is expressed in the coordinates (x_j,y_j) whereas $D^{j+1}_j\,\mathbf{\Phi}^{j+1}$ is expressed in the coordinates (x_{j+1},y_{j+1}). By noting that each point of $\Sigma^j\cap\Omega^{j+1}$ can be represented in the coordinates (x_j,y_j) and (x_{j+1},y_{j+1}) with $x_j=-y_{j+1}=a$ and $y_j=x_{j+1}$ and that each point of $\Sigma^{j+1}\cap\Omega^j$ can be also represented in these coordinates but with $y_j=x_{j+1}=a$ and $x_j=-y_{j+1}$, the relations (43) write as follows*

$$\mathbf{\Phi}^j(a,t) = [D^{j+1}_j\,\mathbf{\Phi}^{j+1}](t,-a), \quad t>a \quad \textit{and} \quad \mathbf{\Phi}^{j+1}(a,t) = [D^j_{j+1}\,\mathbf{\Phi}^j](-t,a), \quad t<-a; \quad j\in[\![0,3]\!].$$

In the isotropic case, one can check that if u is the outgoing solution of (1), then $\mathbf{u}|_{\Omega_b}$ and $\{\mathbf{\Phi}^j := \mathbf{u}\big|_{\Sigma^j},\ j\in[\![0,3]\!]\}$ satisfy Problem (44). But what about the reverse ? There are still many points to elucidate in order to answer this question rigorously and positively in the case of interest, namely the case where $\omega\in\mathbb{R}$. But the equivalence can be proved easily when $\Im(\omega^2)>0$, even for the general anisotropic case, following what is done in [46] for scalar problems. Note that if $\Im(\omega^2)>0$, the outgoing solution of (1) is in $\left[H^1(\Omega)\right]^2$. We give below this result and its proof. This gives an insight on why the method works.

Theorem 4.2. *If $\Im(\omega^2)>0$, Problem (44) is equivalent to the original problem (1) in the following sense: if $\mathbf{u}^b\in[H^1(\Omega_b)]^2$ and $\mathbf{\Phi}^j\in[H^{1/2}(\Sigma^j)]^2$, $j\in[\![0,3]\!]$, satisfy (44), then $\mathbf{U}^j(\mathbf{\Phi}^j)=\mathbf{U}^{j+1}(\mathbf{\Phi}^{j+1})$ in $\Omega^j\cap\Omega^{j+1}$ for all $j\in[\![0,3]\!]$. Moreover the function $\mathbf{u}\in[H^1(\Omega)]^2$ defined by $\mathbf{u}|_{\Omega_b}=\mathbf{u}^b$ and $\mathbf{u}|_{\Omega^j}=\mathbf{U}^j(\mathbf{\Phi}^j)$ for all $j\in\mathbb{Z}/4\mathbb{Z}$ is solution of Problem (1).*

Proof. Note first that for all $j \in [\![0,3]\!]$ $\mathbf{\Phi}^j \in [H^{1/2}(\Sigma^j)]^2$ and $\Im(\omega^2) > 0$, $\mathbf{U}^j(\mathbf{\Phi}^j) \in [H^1(\Omega^j)]^2$. Then, the vector field $\mathbf{v}^j = \mathbf{U}^j(\mathbf{\Phi}^j) - \mathbf{U}^{j+1}(\mathbf{\Phi}^{j+1}) \in \left[H^1(\Omega^j \cap \Omega^{j+1})\right]^2$ satisfies the homogeneous equation in the quarter plane $\Omega^j \cap \Omega^{j+1}$

$$-\mathrm{div}\,\sigma(\mathbf{v}^j) - \rho\omega^2\mathbf{v}^j = 0, \text{ in } \Omega^j \cap \Omega^{j+1}, \quad j \in [\![0,3]\!]. \tag{45}$$

Moreover $\mathbf{v}^j$ vanishes on the boundary of $\Omega^j \cap \Omega^{j+1}$ by the last equation of (44) and the definition (42)

$$\left| \begin{array}{l} \mathbf{U}^j(\mathbf{\Phi}^j) - \mathbf{U}^{j+1}(\mathbf{\Phi}^{j+1}) = D^j_{j+1}(\mathbf{\Phi}^j) - \mathbf{\Phi}^{j+1} = 0 \text{ on } \Sigma^{j+1} \cap \Omega^j, \\ \mathbf{U}^j(\mathbf{\Phi}^j) - \mathbf{U}^{j+1}(\mathbf{\Phi}^{j+1}) = \mathbf{\Phi}^j - D^{j+1}_j(\mathbf{\Phi}^{j+1}) = 0 \text{ on } \Sigma^j \cap \Omega^{j+1}, \end{array} \right. , \quad j \in [\![0,3]\!].$$

Integrating by parts, we get (with $\varepsilon(\mathbf{v}^j)$ denoting the strain tensor)

$$\int_{\Omega^j \cap \Omega^{j+1}} \sigma(\mathbf{v}^j) : \overline{\varepsilon(\mathbf{v}^j)} - \rho\omega^2 \int_{\Omega^j \cap \Omega^{j+1}} |\mathbf{v}^j|^2 = 0, \quad j \in [\![0,3]\!].$$

Using (2) and (6), the first integral is real and the hypothesis $\Im(\omega^2) > 0$ ensures that $\mathbf{v}^j$ vanishes in the quarter plane $\Omega^j \cap \Omega^{j+1}$.

Now, since $\mathbf{U}^j(\mathbf{\Phi}^j) = \mathbf{U}^{j+1}(\mathbf{\Phi}^{j+1})$ in $\Omega^j \cap \Omega^{j+1}$, we can define unequivocally a function $\mathbf{u}_{\mathrm{ext}} \in [H^1(\Omega \setminus \Omega_a)]^2$ by $\mathbf{u}_{\mathrm{ext}}|_{\Omega^j} = \mathbf{U}^j(\mathbf{\Phi}^j)$ for all $j \in [\![0,3]\!]$. Moreover, from the definition (37) of $\mathbf{U}^j(\mathbf{\Phi}^j)$ and from (44), we deduce that

$$\left| \begin{array}{lll} \mathbf{u}_{\mathrm{ext}} = \mathbf{\Phi}^j & \text{on} & \Sigma^j_{aa}, \\ \sigma(\mathbf{u}_{\mathrm{ext}})\nu - i\gamma^j\mathbf{u}_{\mathrm{ext}} = \sigma(\mathbf{u}^b)\nu - i\gamma^j\mathbf{u}^b & \text{on} & \Sigma^j_{bb}, \end{array} \right. , \quad j \in [\![0,3]\!].$$

Consequently, $\mathbf{v} = \mathbf{u}^b - \mathbf{u}_{\mathrm{ext}} \in \left[H^1(\Omega_b \setminus \Omega_a)\right]^2$ satisfies

$$\left| \begin{array}{lll} -\mathrm{div}\,\sigma(\mathbf{v}) - \rho\omega^2\mathbf{v} = 0 & \text{in} & \Omega_b \setminus \Omega_a, \\ \mathbf{v} = 0 & \text{on} & \Sigma^j_{aa}, \quad j \in [\![0,3]\!], \\ \sigma(\mathbf{v})\nu^j - i\gamma^j\mathbf{v} = 0. & \text{on} & \Sigma^j_{bb}, \quad j \in [\![0,3]\!]. \end{array} \right. \tag{46}$$

Integrating by parts, we get

$$\int_{\Omega_b \setminus \Omega_a} \sigma(\mathbf{v}) : \overline{\varepsilon(\mathbf{v})} - \omega^2 \int_{\Omega_b \setminus \Omega_a} \rho|\mathbf{v}|^2 - i\sum_{j=0}^{3} \int_{\Sigma^j_{bb}} \gamma^j|\mathbf{v}|^2 = 0. \tag{47}$$

Again, since the first integral is real, the hypothesis $\Im(\omega^2) > 0$ and the fact that the γ^j's are positive definite ensure that $\mathbf{v}$ vanishes in $\Omega_b \setminus \Omega_a$. Finally, the function $\mathbf{u}$ defined by $\mathbf{u}|_{\Omega_b} = \mathbf{u}^b$ and $\mathbf{u}|_{\Omega \setminus \Omega_a} = \mathbf{u}_{\mathrm{ext}}$ is solution of Problem (1). □

If $\omega^2 \in \mathbb{R}^+$, the equivalence raises challenging questions for the following reasons. First, as the solution of (1) decays only like $r^{-1/2}$ as $r := |\mathbf{x}| \to +\infty$, we cannot expect that its traces on the Σ^j's are in $[L^2(\Sigma^j)]^2$. Moreover even if for each j, $\mathbf{U}^j(\mathbf{\Phi}^j)$ is supposed to be an outgoing solution in the half-plane Ω^j, it is not clear that the difference $\mathbf{U}^j(\mathbf{\Phi}^j) - \mathbf{U}^{j+1}(\mathbf{\Phi}^{j+1})$ satisfies an adequate radiation condition in the quarter plane

$\Omega^j \cap \Omega^{j+1}$. Thus, we cannot easily conclude that $\mathbf{U}^j(\mathbf{\Phi}^j) = \mathbf{U}^{j+1}(\mathbf{\Phi}^{j+1})$ in $\Omega^j \cap \Omega^{j+1}$. If we admit this result[1], the end of the proof works well. Indeed, one can still show that the solution of (46) is equal to 0. From (47) with $\omega^2 \in \mathbb{R}^+$, since the γ^j's are positive definite, we deduce that $\mathbf{v} = 0$ on each Σ^j_{bb}. Then the third equation of (46) implies that also $\sigma(\mathbf{v})\nu^j = 0$ on each Σ^j_{bb}. One can then conclude using the unique continuation principle, proved in [4] for the isotropic case and in [97] for some anisotropic materials.

Despite these theoretical difficulties, we conjecture that for a solution $(\mathbf{u}^b, \mathbf{\Phi}^0, \mathbf{\Phi}^1, \mathbf{\Phi}^2, \mathbf{\Phi}^3)$ of (44), the outgoing half-space solutions $\mathbf{U}^j(\mathbf{\Phi}^j)$ coincide where they coexist. Then the function $\mathbf{u} \in [H^1_{\text{loc}}(\Omega)]^2$ given by $\mathbf{u}|_{\Omega_b} = \mathbf{u}^b$ and for each j, $\mathbf{u}|_{\Omega^j} = \mathbf{U}^j(\mathbf{\Phi}^j)$ is well defined and is, for the anisotropic case, our definition of the *outgoing* solution of Problem (1).

4.2. Half-space representation in the isotropic case

Let us now describe how to get an analytical representation of the solution in each half-space in terms of its trace. Namely, let for all $\mathbf{\Phi}$ determine $\mathbf{U}^j(\mathbf{\Phi})$ the outgoing solution of (37) where $\sigma(\mathbf{U}^j)$ is linked to the displacement field by the Hooke's law (5) in the isotropic case (9) and where by (7), the coefficients ρ, λ and μ are constant in Ω^j. The meaning of *outgoing* is given below. To simplify the notation, we will focus first on the case $j = 0$ and on the half-space Ω^0 where the local coordinates (x_0, y_0) coincide with the global ones (x, y).

To express analytically $\mathbf{U}^0(\mathbf{\Phi})$ in terms of its trace $\mathbf{\Phi}$, we take advantage of the homogeneity of the medium and apply formally a Fourier transform in the direction of the boundary, *i.e.* the $y-$direction. In the sequel, we will consider the following definition of the Fourier transformation $\hat{f}$ of a function f

$$\hat{f}(\xi) = \frac{1}{\sqrt{2\pi}} \int_{\mathbb{R}} f(y) e^{-i\xi y} dy,$$

so that the inverse Fourier transform is given by

$$f(y) = \frac{1}{\sqrt{2\pi}} \int_{\mathbb{R}} \hat{f}(\xi) e^{i\xi y} d\xi.$$

Denoting by $\hat{\mathbf{U}}^0$ the Fourier transformation in the $y-$direction of $\mathbf{U}^0$ (we forget the dependence with respect to the Dirichlet data $\mathbf{\Phi}$ for now), we get that $\hat{\mathbf{U}}^0$ satisfies

$$\left(-\partial^2_{xx} \begin{bmatrix} \lambda + 2\mu & 0 \\ 0 & \mu \end{bmatrix} - i\xi\partial_x \begin{bmatrix} 0 & \lambda + \mu \\ \lambda + \mu & 0 \end{bmatrix} + \xi^2 \begin{bmatrix} \mu & 0 \\ 0 & \lambda + 2\mu \end{bmatrix} - \rho\omega^2 \right) \begin{bmatrix} \hat{\mathbf{U}}^0_x \\ \hat{\mathbf{U}}^0_y \end{bmatrix} = \begin{bmatrix} 0 \\ 0 \end{bmatrix} \tag{48}$$

which turns to be a system of two coupled ordinary differential equations of order 2 where the Fourier variable ξ plays the role of a parameter. It is well known that the general solution of such system can

[1]Note that for the Helmholtz equation, the equivalence between the HSM formulation and the equation was proven for $\omega \in \mathbb{R}$ provided the traces satisfy a radiation condition at infinity, which is analogous to the standard Sommerfeld radiation condition [24].

be expressed in terms of the particular solutions of the form $e^{i\kappa x}\mathbf{V}$, where the κ's are the roots of the characteristic polynomial of the system. This characteristic polynomial is given here by

$$P_\xi(\kappa) := \mathcal{F}(\kappa, \xi, \omega),$$

where $\mathcal{F}$ is defined by (17). Note that contrary to Section 3, the parameter κ can take complex values. Since here

$$\mathcal{A}(\kappa, \xi) = \kappa^2 \begin{bmatrix} c_P^2 & 0 \\ 0 & c_S^2 \end{bmatrix} + \kappa\xi \begin{bmatrix} 0 & c_P^2 - c_S^2 \\ c_P^2 - c_S^2 & 0 \end{bmatrix} + \xi^2 \begin{bmatrix} c_S^2 & 0 \\ 0 & c_P^2 \end{bmatrix}, \tag{49}$$

c_P and c_S being defined in (11), $P_\xi(\cdot)$ can be expressed as

$$P_\xi(\kappa) = c_P^2 c_S^2 \left(\kappa^2 + \xi^2 - \frac{\omega^2}{c_P^2}\right)\left(\kappa^2 + \xi^2 - \frac{\omega^2}{c_S^2}\right). \tag{50}$$

For each $\xi \in \mathbb{R}$, the four roots of P_ξ are then $\pm\kappa_P(\xi)$ and $\pm\kappa_S(\xi)$ where

$$\kappa_I(\xi) := \begin{vmatrix} \sqrt{k_I^2 - \xi^2} & \text{if } |\xi| \le k_I \\ i\sqrt{\xi^2 - k_I^2} & \text{if } |\xi| \ge k_I \end{vmatrix} \tag{51}$$

with $k_I = \omega/c_I$ for $I \in \{P, S\}$. By using the convention $\Im(\sqrt{z}) \ge 0$, $z \in \mathbb{C} \setminus \mathbb{R}^+$, κ_I can be simply defined as $\kappa_I(\xi) = \sqrt{k_I^2 - \xi^2}$. Finally, for $\xi \notin \{\pm k_P, \pm k_S\}$, the general form of a solution of the system (48) is given by

$$A_{P,+}(\xi)\mathbf{P}_+(\xi)e^{i\kappa_P(\xi)(x-a)} + A_{P,-}(\xi)\mathbf{P}_-(\xi)e^{-i\kappa_P(\xi)(x-a)} + A_{S,+}(\xi)\mathbf{S}_+(\xi)e^{i\kappa_S(\xi)(x-a)} + A_{S,-}(\xi)\mathbf{S}_-(\xi)e^{-i\kappa_S(\xi)(x-a)}$$

where $A_{P,\pm}(\xi)$ and $A_{S,\pm}(\xi)$ are complex coefficients, and where $\mathbf{P}_\pm(\xi)$ and $\mathbf{S}_\pm(\xi)$ are eigenvectors of $\mathcal{A}(\pm\kappa_P, \xi)$ and $\mathcal{A}(\pm\kappa_S, \xi)$ associated to the eigenvalue ω^2 that can be chosen as

$$\mathbf{P}_\pm(\xi) = \begin{bmatrix} \pm\kappa_P(\xi) \\ \\ \xi \end{bmatrix} \text{ and } \mathbf{S}_\pm(\xi) = \begin{bmatrix} \xi \\ \\ \mp\kappa_S(\xi) \end{bmatrix}. \tag{52}$$

When $|\xi| < k_I$, $I = P$ or $I = S$, the terms above correspond (after multiplication by the factor $e^{i\xi y}$ of the inverse Fourier transform) to propagative plane waves:

$$\mathbf{P}_\pm(\xi)e^{i(\pm\kappa_P(\xi)(x-a)+\xi y)}, \quad \text{or} \quad \mathbf{S}_\pm(\xi)e^{i(\pm\kappa_S(\xi)(x-a)+\xi y)},$$

since by definition of $\kappa_I(\xi)$, $\mathcal{F}(\pm\kappa_I(\xi), \xi, \omega) = 0$ (where the dispersion relation is given by (17), or by (22) for isotropic materials). One speaks of P waves (or pressure waves) when $I = P$, and of S waves (or shear waves), when $I = S$. As is well-known, P waves are longitudinal waves and S waves are transverse waves.

To go further, we determine the outgoing solution of (37) as follows.

- First, the solution has to be bounded when x tends to $+\infty$. Since if $|\xi| > k_I$ for $I \in \{P, S\}$, $x \mapsto e^{-i\kappa_I(\xi)(x-a)}$ is exponentially growing, one has necessarily

$$A_{P,-}(\xi) = 0 \quad \text{if } |\xi| > k_P, \text{ and } \quad A_{S,-}(\xi) = 0 \quad \text{if } |\xi| > k_S.$$

- Besides, if $|\xi| < k_I$ for $I \in \{P, S\}$, only the plane wave which propagates towards $x \to +\infty$ is physically relevant. Using the discussion of Section 3 (in the isotropic case, group and phase velocities coincide), we can easily check that this corresponds if $|\xi| < k_P$ to select the one of amplitude $A_{P,+}(\xi)$ and to impose $A_{P,-}(\xi) = 0$. Similarly, if $|\xi| < k_S$, we impose $A_{S,-}(\xi) = 0$.

To conclude, $\hat{\mathbf{U}}^0(\cdot, \xi)$ writes as

$$\hat{\mathbf{U}}^0(x, \xi) = A_{P,+}(\xi)\mathbf{P}_+(\xi)e^{i\kappa_P(\xi)(x-a)} + A_{S,+}(\xi)\mathbf{S}_+(\xi)e^{i\kappa_S(\xi)(x-a)}, \quad x > a,\ \xi \in \mathbb{R}.$$

We say that the inverse Fourier transform of $\hat{\mathbf{U}}^0$ is the *outgoing* solution of (48), because we have selected outgoing plane waves in its representation.

Then, from (37), we have that $\hat{\mathbf{U}}^0(a, \xi) = \hat{\mathbf{\Phi}}(\xi)$ which enables to determine $A_{P,+}(\xi)$ and $A_{S,+}(\xi)$ in terms of $\hat{\mathbf{\Phi}}(\xi)$. More precisely, by using the definition (52) of $\mathbf{P}_+(\xi)$ and $\mathbf{S}_+(\xi)$ we have

$$Q(\xi)\begin{bmatrix} A_{P,+}(\xi) \\ A_{S,+}(\xi) \end{bmatrix} = \hat{\mathbf{\Phi}}(\xi) \quad \text{where } Q(\xi) = \begin{bmatrix} \kappa_P(\xi) & \xi \\ \xi & -\kappa_S(\xi) \end{bmatrix}. \tag{53}$$

We easily check that since $\omega \neq 0$, $Q(\xi)$ is invertible and the matrix $Q^{-1}(\xi)$ corresponds to the projection on the basis of eigenvectors $\mathbf{P}_+(\xi)$ and $\mathbf{S}_+(\xi)$.

Finally, one can apply the inverse Fourier transform to find that for all $\mathbf{\Phi}$, the outgoing solution of (37) is given by

$$\mathbf{U}^0(\mathbf{\Phi})(x, y) = \frac{1}{\sqrt{2\pi}} \int_{\mathbb{R}} Q(\xi)e^{i(K(\xi)(x-a)+\xi y)}Q(\xi)^{-1}\hat{\mathbf{\Phi}}(\xi)\, d\xi, \quad x > a,\ y \in \mathbb{R}, \tag{54}$$

where $Q(\xi)$ is defined in (53) and

$$K(\xi) := \begin{bmatrix} \kappa_P(\xi) & 0 \\ 0 & \kappa_S(\xi) \end{bmatrix}, \tag{55}$$

with $\kappa_P(\xi)$ and $\kappa_S(\xi)$ defined by (51). Note that here and in the sequel, the notation with the exponential in (54) has to be understood as follows:

$$e^{i(K(\xi)(x-a)+\xi y)} := \begin{bmatrix} e^{i(\kappa_P(\xi)(x-a)+\xi y)} & 0 \\ 0 & e^{i(\kappa_S(\xi)(x-a)+\xi y)} \end{bmatrix}.$$

One can easily deduce similar expressions for the half-space representations in Ω^j, for $j = 1$, 2 or 3, the coordinates (x, y) being replaced by the local ones (x_j, y_j), but keeping the components of the vector fields $\mathbf{U}^j(\mathbf{\Phi})$ and $\mathbf{\Phi}$ in the global coordinate system (x, y). This is achieved through the application of the rotation matrix $\mathcal{R}(\theta_j)$ defined in (31).

Proposition 4.3. *Consider an isotropic material satisfying* (5) *and* (9). *Then, for all* $j \in [\![0, 3]\!]$, *the outgoing solution of* (37) *is given by*

$$\mathbf{U}^j(\mathbf{\Phi})(x_j, y_j) = \frac{1}{\sqrt{2\pi}} \int_{\mathbb{R}} \mathcal{R}(\theta_j)^{-1}\, Q(\xi)e^{i(K(\xi)(x_j-a)+\xi y_j)}Q(\xi)^{-1}\, \mathcal{R}(\theta_j)\, \hat{\mathbf{\Phi}}(\xi)\, d\xi,\ x_j > a,\ y_j \in \mathbb{R}, \tag{56}$$

where $\mathcal{R}(\theta_j)$ *is defined in* (31), $Q(\xi)$ *in* (53) *and* $K(\xi)$ *in* (55).

A straightforward consequence is given by the following corollary.

Corollary 4.4. *With the hypotheses of the previous lemma, the operators $D^j_{j\pm1}$ defined by* (42) *have the following expression*

$$D^j_{j\pm1}(\mathbf{\Phi})(x_j,\pm a)=\frac{1}{\sqrt{2\pi}}\int_{\mathbb{R}}\ \mathcal{R}(\theta_j)^{-1}\,Q(\xi)e^{i(K(\xi)(x_j-a)\pm\xi a)}Q^{-1}(\xi)\,\mathcal{R}(\theta_j)\,\hat{\mathbf{\Phi}}(\xi)\,d\xi,\ x_j>a. \tag{57}$$

Let us now derive the expression of the operators Λ^j defined in (40). Again we begin with the case $j=0$. Since $\nu^0=\mathbf{e}_x$ and using (5) and (9), we have

$$\sigma(\mathbf{U}^0(\mathbf{\Phi}))\nu^0=\begin{bmatrix}\sigma_{xx}(\mathbf{U}^0(\mathbf{\Phi}))\\ \sigma_{xy}(\mathbf{U}^0(\mathbf{\Phi}))\end{bmatrix}=\begin{bmatrix}(\lambda+2\mu)\partial_x & \lambda\partial_y\\ \mu\partial_y & \mu\partial_x\end{bmatrix}\mathbf{U}^0(\mathbf{\Phi}). \tag{58}$$

Then, due to the isotropy and to the definition of the local coordinates (x_j,y_j), we deduce:

$$[\mathcal{R}(\theta_j)\sigma(\mathbf{U}^j(\mathbf{\Phi}))\nu^j]=\begin{bmatrix}(\lambda+2\mu)\partial_{x_j} & \lambda\partial_{y_j}\\ \mu\partial_{y_j} & \mu\partial_{x_j}\end{bmatrix}\mathcal{R}(\theta_j)\mathbf{U}^j(\mathbf{\Phi}),\quad j\in[\![0,3]\!].$$

Therefore, using now the expression (56) of $\mathbf{U}^j(\mathbf{\Phi})$ we deduce the expression of the operator Λ^j.

Proposition 4.5. *Consider an isotropic material satisfying* (5) *and* (9). *Then the field $\mathbf{T}^j(\mathbf{\Phi})$ defined by*

$$\mathbf{T}^j(\mathbf{\Phi})(x_j,y_j):=\sigma(\mathbf{U}^j(\mathbf{\Phi}))(x_j,y_j)\nu^j,\ x_j>a,\ y_j\in\mathbb{R},\quad j\in[\![0,3]\!] \tag{59}$$

is given by

$$\mathbf{T}^j(\mathbf{\Phi})(x_j,y_j)=\frac{1}{\sqrt{2\pi}}\int_{\mathbb{R}}\mathcal{R}(\theta_j)^{-1}F(\xi)e^{i(K(\xi)(x_j-a)+\xi y_j)}Q(\xi)^{-1}\,\mathcal{R}(\theta_j)\,\hat{\mathbf{\Phi}}(\xi)\,d\xi,\ y_j\in\mathbb{R},\quad j\in[\![0,3]\!] \tag{60}$$

where $\mathcal{R}(\theta_j)$ is defined in (31), *$Q(\xi)$ by* (53), *$K(\xi)$ by* (55) *and*

$$F(\xi):=i\begin{bmatrix}\lambda+2\mu & 0\\ 0 & \mu\end{bmatrix}Q(\xi)K(\xi)+i\xi\begin{bmatrix}0 & \lambda\\ \mu & 0\end{bmatrix}Q(\xi).$$

By definition of the operators Λ^j (see (40)), one has

$$\Lambda^j(\mathbf{\Phi})(b,y_j)=\mathbf{T}^j(\mathbf{\Phi})(b,y_j)-i\gamma^j\mathbf{U}^j(\mathbf{\Phi})(b,y_j),\ y_j\in(-b,b),\quad j\in[\![0,3]\!]. \tag{61}$$

A straightforward consequence of the previous lemma is then given by the corollary.

Corollary 4.6. *With the hypotheses of the previous lemma, the operators Λ^j defined by* (40) *have the following expression :*

$$\Lambda^j(\mathbf{\Phi})(b,y_j)=\frac{1}{\sqrt{2\pi}}\int_{\mathbb{R}}\mathcal{R}(\theta_j)^{-1}\left[F(\xi)-i\gamma^jQ(\xi)\right]e^{i(K(\xi)(b-a)+\xi y_j)}Q(\xi)^{-1}\,\mathcal{R}(\theta_j)\,\hat{\mathbf{\Phi}}(\xi)\,d\xi,\ y_j\in(-b,b),\ j\in[\![0,3]\!]. \tag{62}$$

4.3. Half-space representation in the anisotropic case

For the anisotropic case, we follow the same approach than in the previous section. Here $\sigma(\mathbf{U}^j)$ is linked to the displacement field thanks to the general anisotropic Hooke's law (5). We focus first on the half-space Ω^0 ($j = 0$). Again, we apply a Fourier transform in the y-direction to the equation, in order to derive the expression of the Fourier transform of the outgoing half-space solution. This will clarify the definition of what means "outgoing" in the anisotropic case.

The Fourier transform $\hat{\mathbf{U}}^0$ of $\mathbf{U}^0$ (we forget the dependence with respect to the Dirichlet data $\mathbf{\Phi}$ for now) satisfies

$$\left(-\partial_{xx}^2 \mathcal{A}_0 - i\xi\partial_x[\mathcal{A}_1 + \mathcal{A}_1{}^{\mathrm{T}}] + \xi^2 \mathcal{A}_2 - \rho^\infty \omega^2\right) \hat{\mathbf{U}}^0 = 0, \tag{63}$$

where $\mathcal{A}_0$, $\mathcal{A}_1$ and $\mathcal{A}_2$ are given in (15). The differential system (63) is, as in the previous section, a system of two coupled ordinary differential equations of order 2, parametrized by the Fourier variable ξ. Again, the characteristic polynomial of the system is given by

$$P_\xi(\kappa) := \mathcal{F}(\kappa, \xi, \omega), \tag{64}$$

where $\mathcal{F}$ is defined by (17) and

$$\mathcal{A}(\kappa, \xi) = \frac{1}{\rho}\left[\kappa^2 \mathcal{A}_0 + \kappa\xi(\mathcal{A}_1 + \mathcal{A}_1{}^{\mathrm{T}}) + \xi^2 \mathcal{A}_2\right].$$

The computation of the roots of the characteristic polynomial is less explicit than in the isotropic case. But we can state several general properties of these roots.

As a polynomial of degree 4, P_ξ has at most four distinct roots. Moreover, since the coefficients of the polynomial P_ξ are real, one has

$$\forall \xi \in \mathbb{R},\ \forall \kappa \in \mathbb{C},\ P_\xi(\kappa) = P_{-\xi}(-\kappa) = \overline{P_\xi(\overline{\kappa})}. \tag{65}$$

As a consequence, if $\kappa \in \mathbb{C}$ is a root of P_ξ, then $\overline{\kappa}$ is too, and $-\kappa$ is a root of $P_{-\xi}$. Note that for orthotropic materials, if κ is a root of P_ξ, then $-\kappa$ is too.

Concerning the real roots of P_ξ, we can use the description done in Section 3. Indeed, when $\kappa \in \mathbb{R}$ is a root of P_ξ, $(\kappa/\omega, \xi/\omega)$ belongs to the slowness diagram $\mathcal{S}$ defined by (25). This allows in particular to introduce

$$k_* = \inf\{\, k > 0,\ \ \forall \xi \in \mathbb{R},\ \ |\xi| > k, \quad P_\xi \ \text{ has no real roots}\} \ \ < \ \ +\infty. \tag{66}$$

Using Section 3 and Appendix B, we can show the following result.

Proposition 4.7. *For a.e. $\xi \in \mathbb{R}$, P_ξ has four distinct roots and*

- *if $|\xi| < k_*$, P_ξ has either two or four real roots,*
- *if $|\xi| > k_*$, P_ξ has four non real roots.*

For any κ, such that $P_\xi(\kappa) = 0$, we denote $\mathbf{V}_\kappa(\xi)$ an eigenvector of $\mathcal{A}(\kappa, \xi)$ associated to the eigenvalue ω^2. Since for a.e. ξ, the roots are simple, the general form of a solution of the system (63) is given by

$$\sum_{\kappa, P_\xi(\kappa)=0} A_\kappa(\xi)\mathbf{V}_\kappa(\xi)e^{i\kappa(x-a)}, \tag{67}$$

where the $A_\kappa(\xi)$'s are complex coefficients. We describe how to construct outgoing solution of (63) for a.e. ξ.

- If κ with $\Im(\kappa) > 0$ is a root of P_ξ then, as explained just above, $\overline{\kappa}$ is also. The solution has to be bounded when x tends to $+\infty$. This implies that one has necessarily $A_{\overline{\kappa}}(\xi) = 0$, since $x \mapsto e^{i\overline{\kappa}(x-a)}$ is exponentially growing at $+\infty$.

- If $\kappa \in \mathbb{R}$ is a root of P_ξ, the term $A_\kappa(\xi)\mathbf{V}_\kappa e^{i\kappa(x-a)}$ leads to a plane wave contribution after inverse Fourier transform. To select outgoing contributions, *i.e.* plane waves which propagate towards $x \to +\infty$, following Section 3, one can rely on the sign of the energy flux. Setting $\mathbf{u}(x, y) = \mathbf{V}_\kappa e^{i(\kappa(x-a)+\xi y)}$, we impose $A_\kappa(\xi) = 0$ if $\mathbf{u}$ is ingoing, *i.e.* if it satisfies $\Im(\sigma(\mathbf{u})\mathbf{e_x} \cdot \bar{\mathbf{u}}) < \mathbf{0}$.

  Note that, unlike the isotropic case, this selection may lead to a negative κ, see Section 3 and Figures 1, 2. Such plane wave is said to be backward in the $x-$direction.

One can check[2] that for almost every ξ, with this process of selection, there remain only two terms in (67), that we call outgoing waves (the two others that have been removed correspond to ingoing waves). We denote by $\kappa_1^0(\xi)$ and $\kappa_2^0(\xi)$ the two roots of P_ξ corresponding to outgoing waves. The two roots can be chosen so that $\xi \mapsto \kappa_1^0(\xi)$ and $\kappa_2^0(\xi)$ are piecewise continuous. We denote $\mathbf{V}_i^0(\xi)$, $i \in \{1, 2\}$ an eigenvector of $\mathcal{A}(\kappa_i^0(\xi), \xi)$ associated to the eigenvalue ω^2. This eigenvector can also be chosen so that $\xi \mapsto \mathbf{V}_i^0(\xi)$ is piecewise continuous. Consequently, an outgoing solution of the half-space problem in the anisotropic case writes as

$$A_1^0(\xi)\mathbf{V}_1^0(\xi)e^{i\kappa_1^0(\xi)(x-a)} + A_2^0(\xi)\mathbf{V}_2^0(\xi)e^{i\kappa_2^0(\xi)(x-a)}.$$

Besides, we have that $\hat{\mathbf{U}}^0(\xi) = \hat{\mathbf{\Phi}}(\xi)$ at $x = a$, which can be written as follows:

$$Q^0(\xi)\begin{bmatrix} A_1^0(\xi) \\ A_2^0(\xi) \end{bmatrix} = \hat{\mathbf{\Phi}}(\xi) \quad \text{where } Q^0(\xi) := \begin{bmatrix} \mathbf{V}_1^0(\xi) & \mathbf{V}_2^0(\xi) \end{bmatrix}. \tag{68}$$

We show in Appendix C that for a.e. ξ, $\mathbf{V}_1^0(\xi)$ and $\mathbf{V}_2^0(\xi)$ are linearly independent, so that $Q^0(\xi)$ is invertible. This enables to determine $A_1^0(\xi)$ and $A_2^0(\xi)$ in terms of $\hat{\mathbf{\Phi}}(\xi)$. Finally, one can apply the inverse

[2]This can be proved first for $\omega_\varepsilon = \omega + i\varepsilon$ with $\varepsilon > 0$ where equation (63) always admits two solutions in L^2, and then by passing to the limit $\varepsilon \to 0$. This can also be proved by geometrical arguments on the slowness curve.

Fourier transform to find that for all $\mathbf{\Phi}$, the outgoing solution of the half-space problem set in Ω^0 is given by

$$\mathbf{U}^0(\mathbf{\Phi})(x,y) = \frac{1}{\sqrt{2\pi}} \int_{\mathbb{R}} Q^0(\xi) e^{i(K^0(\xi)(x-a)+\xi y)} Q^0(\xi)^{-1} \hat{\mathbf{\Phi}}(\xi)\, d\xi, \quad x > a,\ y \in \mathbb{R} \tag{69}$$

where $Q^0(\xi)$ is defined in (68) and

$$K^0(\xi) := \begin{bmatrix} \kappa_1^0(\xi) & 0 \\ 0 & \kappa_2^0(\xi) \end{bmatrix}. \tag{70}$$

Unlike the isotropic case, the representation of the other half-space solutions cannot be deduced directly from this one, by a simple rotation. One has to apply the same approach to derive the expression of the solution in each half-space. First, for the half-space solution $\mathbf{U}^2(\mathbf{\Phi})$, it suffices to notice that the characteristic polynomial that we denote P_ξ^2 is equal to $P_{-\xi}$ where P_ξ is the characteristic polynomial defined in (64). Moreover since $x_2 = -x_0$, it is easy to see that the roots which are not selected to express the outgoing solution in Ω^0 have to be selected to define the outgoing solution in Ω^2 (in other words, thanks to (65), an ingoing wave in Ω^0 corresponds to an outgoing wave in Ω^2). For the half-space solution $\mathbf{U}^1(\mathbf{\Phi})$, one has to use the same reasoning than for $\mathbf{U}^0(\mathbf{\Phi})$: compute the roots of the characteristic polynomial (which has no links in general with P_ξ defined in (64)) and select the "good" roots in order to obtain an outgoing solution. Finally, for the expression of $\mathbf{U}^3(\mathbf{\Phi})$, it suffices to use the computations already done for $\mathbf{U}^1(\mathbf{\Phi})$ applying the same reasoning that we have used to express $\mathbf{U}^2(\mathbf{\Phi})$ by using the computations already done for $\mathbf{U}^0(\mathbf{\Phi})$. For all j, we denote by $\kappa_1^j(\xi)$ and $\kappa_2^j(\xi)$ the roots defining outgoing waves in Ω^j and by $\mathbf{V}_1^j(\xi)$ and $\mathbf{V}_2^j(\xi)$ associated eigenvectors. Then we set

$$Q^j(\xi) := \begin{bmatrix} \mathbf{V}_1^j(\xi) & \mathbf{V}_2^j(\xi) \end{bmatrix} \text{ and } K^j(\xi) := \begin{bmatrix} \kappa_1^j(\xi) & 0 \\ 0 & \kappa_2^j(\xi) \end{bmatrix}, \quad j \in [\![0,3]\!] \tag{71}$$

and we have the

Lemma 4.8. *Consider an anisotropic material satisfying* (5)*. The outgoing solution of* (37) *is given by*

$$\mathbf{U}^j(\mathbf{\Phi})(x_j,y_j) = \frac{1}{\sqrt{2\pi}} \int_{\mathbb{R}} \mathcal{R}(\theta_j)^{-1}\, Q^j(\xi) e^{i(K^j(\xi)(x_j-a)+\xi y_j)} Q^j(\xi)^{-1}(\xi)\, \mathcal{R}(\theta_j)\, \hat{\mathbf{\Phi}}(\xi)\, d\xi,\ x_j > a,\ y_j \in \mathbb{R},\ j \in [\![0,3]\!] \tag{72}$$

where $\mathcal{R}(\theta_j)$ is defined in (31) *and $Q^j(\xi)$ and $K^j(\xi)$ by* (71)*.*

A consequence is given by the

Corollary 4.9. *With the hypotheses and notations of the previous lemma, the operators $D_{j\pm1}^j$ defined by* (42) *have the following expression:*

$$D_{j\pm1}^j(\mathbf{\Phi})(x_j,\pm a) = \frac{1}{\sqrt{2\pi}} \int_{\mathbb{R}} \mathcal{R}(\theta_j)^{-1}\, Q^j(\xi) e^{i(K^j(\xi)(x_j-a)\pm\xi a)} Q^j(\xi)^{-1}\, \mathcal{R}(\theta_j)\, \hat{\mathbf{\Phi}}(\xi)\, d\xi,\ x_j > a,\ j \in [\![0,3]\!] \tag{73}$$

and the operators Λ^j *defined by* (40) *have the following expression:*

$$\Lambda^j(\mathbf{\Phi})(b,y_j) = \frac{1}{\sqrt{2\pi}}\int_{\mathbb{R}} \mathcal{R}(\theta_j)^{-1}\,\left[F^j(\xi) - i\gamma^j Q^j(\xi)\right] e^{i(K^j(\xi)(b-a)+\xi y_j)} Q^j(\xi)^{-1}\,\mathcal{R}(\theta_j)\,\hat{\mathbf{\Phi}}(\xi)\,d\xi,\ y_j\in(-b,b),\ j\in[\![0,3]\!] \tag{74}$$

where $F^j(\xi)$ *is defined in Appendix D.*

5. Numerical aspects

5.1. Discretization of the HSM formulation

Let us explain now how to compute a finite element approximation of the solution $(\mathbf{u}^b, \mathbf{\Phi}^0, \mathbf{\Phi}^1, \mathbf{\Phi}^2, \mathbf{\Phi}^3)$ of the HSM system (44). To get a discrete problem, we use several ingredients

- Since the traces are regular functions, their Fourier transforms decay rapidly. As a consequence, we truncate the integrals appearing in the definition of $D^j_{j\pm1}$ (see (57) for the isotropic case and (73) for the anisotropic case) and in the definition of Λ^j (see (62) for the isotropic case and (74) for the anisotropic one). More precisely, the integrals for $\xi\in\mathbb{R}$ are replaced by integrals for $\xi\in(-\hat{\ell},\hat{\ell})$ for some $\hat{\ell}\in\mathbb{R}^+$ chosen such that all propagative waves are at least taken into account, *i.e.* $\hat{\ell} > k_S$ in the isotropic case (see (23) for the definition of k_S) and $\hat{\ell} > k_*$ in the anisotropic case (see (66) for the definition of k_*). Moreover, quadrature formulae are used to evaluate the Fourier integrals. We use a Gauss quadrature rule with q points in a mesh of size $\hat{h}$ of $(-\hat{\ell},\hat{\ell})$. We denote $D^j_{j\pm1,\hat{\mathbf{h}}}$, with $\hat{\mathbf{h}} = (\hat{\ell},\hat{h},q)$, the approximation of $D^j_{j\pm1}$ and $\Lambda^j_{\hat{\mathbf{h}}}$ the approximation of Λ^j. For instance, for the isotropic case we have for all $\mathbf{\Phi}$

$$D^j_{j\pm1,\hat{\mathbf{h}}}(\mathbf{\Phi})(x_j,\pm a) = \frac{1}{\sqrt{2\pi}}\sum_{(\hat{\xi},\hat{w})\in\mathcal{Q}} \hat{w}\,\mathcal{R}(\theta_j)^{-1}\,Q(\hat{\xi})e^{i(K(\hat{\xi})(x_j-a)\pm\hat{\xi}a)}Q^{-1}(\hat{\xi})\,\mathcal{R}(\theta_j)\,\hat{\mathbf{\Phi}}(\hat{\xi}) \tag{75}$$

  where $\mathcal{R}(\theta_j)$ is defined in (31), $Q(\xi)$ in (53) and $K(\xi)$ in (55) and where

$$\mathcal{Q} = \{(\hat{\xi},\hat{w}), \hat{\xi} = -\hat{\ell} + (i-\frac{1}{2})\hat{h} + \frac{\hat{h}}{2}x_j,\ \hat{w} = \frac{\hat{h}}{2}w_j, i\in[\![1,\hat{N}]\!],\ j\in[\![1,q]\!]\}$$

  where $\hat{h} = 2\hat{\ell}/\hat{N}$ and $\{(x_j,w_j), j\in[\![1,q]\!]\}$ correspond to the quadrature rule in $[-1,1]$.

- We introduce a finite dimensional subspace $\mathbf{V}^b_{\mathbf{h}}$ of $H^1(\Omega_b)^2$ for the approximation of the "volume" unknown $\mathbf{u}^b$, and finite dimensional spaces $\mathbf{V}^j_{\mathbf{h^j}}$ for the approximation of the "surface" unknowns $\mathbf{\Phi}^j$. To build the discrete spaces, we use classical 2D Lagrange finite elements for $\mathbf{V}^b_{\mathbf{h}}$ and 1D Lagrange finite elements for each $\mathbf{V}^j_{\mathbf{h^j}}$, $j=[\![0,3]\!]$. More precisely, we introduce a 2D triangular mesh of Ω_b and for $\mathbf{h}=(h,p)$, we denote by $\mathbf{V}^b_{\mathbf{h}}$ the set of continuous vector fields in Ω_b whose components are polynomials functions of degree p in each triangle of the mesh, whose maximal element diameter is denoted h. Concerning $\mathbf{V}^j_{\mathbf{h^j}}$ with $\mathbf{h^j} = (h^j,p^j,\ell^j)$, we first truncate the infinite line Σ^j, $\Sigma^j_{\ell^j} = \{x^j=a\}\times\{|y^j|\le\ell^j\}$

(with $\ell^j > b$) and introduce a 1D mesh of this segment. The space $\mathbf{V}^j_{\mathbf{h^j}}$ is the set of continuous vector fields in Σ^j supported in $\Sigma^j_{\ell^j}$, whose components are polynomials functions of degree p^j in each segment of the mesh, whose maximal element length is denoted h^j.

Let us now derive the equations that should satisfy the discrete solution $(\mathbf{u}^b_h, \mathbf{\Phi}^0_h, \mathbf{\Phi}^1_h, \mathbf{\Phi}^2_h, \mathbf{\Phi}^3_h)$. First the compatibility equations corresponding to the two last lines of (44) can be written in a weak discretized form as follows. For all $j \in \mathbb{Z}/4\mathbb{Z}$ and for all test functions $\mathbf{\Psi}^j_h \in \mathbf{V}^j_h$, we impose:

$$\int_{\Sigma^j} \mathbf{\Phi}^j_h \cdot \overline{\mathbf{\Psi}^j_h} = \int_{\Sigma^j_{aa}} \mathbf{u}^b_h \cdot \overline{\mathbf{\Psi}^j_h} + \int_{\Sigma^j \cap \Omega^{j-1}} D^{j-1}_{j,\hat{\mathbf{h}}}(\mathbf{\Phi}^{j-1}_h) \cdot \overline{\mathbf{\Psi}^j_h} + \int_{\Sigma^j \cap \Omega^{j+1}} D^{j+1}_{j,\hat{\mathbf{h}}}(\mathbf{\Phi}^{j+1}_h) \cdot \overline{\mathbf{\Psi}^j_h}. \tag{76}$$

Note that all integrals are well-defined since $\mathbf{\Psi}^j_h$ has a compact support. Besides, a weak form of the three first lines of (44) is obtained classically. This leads finally to this following discrete version of the HSM problem (44):

Find $(\mathbf{u}^b_h, \mathbf{\Phi}^0_h, \mathbf{\Phi}^1_h, \mathbf{\Phi}^2_h, \mathbf{\Phi}^3_h) \in \mathbf{V}^b_{\mathbf{h}} \times \mathbf{V}^0_{\mathbf{h^0}} \times \mathbf{V}^1_{\mathbf{h^1}} \times \mathbf{V}^2_{\mathbf{h^2}} \times \mathbf{V}^3_{\mathbf{h^3}}$ such that

$\forall (\mathbf{v}^b_h, \mathbf{\Psi}^0_h, \mathbf{\Psi}^1_h, \mathbf{\Psi}^2_h, \mathbf{\Psi}^3_h) \in \mathbf{V}^b_{\mathbf{h}} \times \mathbf{V}^0_{\mathbf{h^0}} \times \mathbf{V}^1_{\mathbf{h^1}} \times \mathbf{V}^2_{\mathbf{h^2}} \times \mathbf{V}^3_{\mathbf{h^3}}$,

$$\left| \begin{array}{rcl} \mathfrak{A}(\mathbf{u}^b_h, \mathbf{v}^b_h) + \displaystyle\sum_{j=0}^{3} \mathfrak{B}^j_{\hat{\mathbf{h}}}(\mathbf{\Phi}^j_h, \mathbf{v}^b_h) & = & \displaystyle\int_{\partial\mathcal{O}} \sigma(\mathbf{u}^{inc})\nu \cdot \overline{\mathbf{v}^b_h}, \\ \displaystyle\sum_{j=0}^{3} \left[\mathfrak{C}^j(\mathbf{u}^b_h, \mathbf{\Psi}^j_h) + \left(\int_{\Sigma^j} \mathbf{\Phi}^j_h \cdot \overline{\mathbf{\Psi}^j_h} \right) + \mathfrak{D}^{j-1}_{j,\hat{\mathbf{h}}}(\mathbf{\Phi}^{j-1}_h, \mathbf{\Psi}^j_h) + \mathfrak{D}^{j+1}_{j,\hat{\mathbf{h}}}(\mathbf{\Phi}^{j+1}_h, \mathbf{\Psi}^j_h) \right] & = & 0, \end{array} \right. \tag{77}$$

where the various sesquilinear forms are defined below:

for $(\mathbf{u}^b_h, \mathbf{\Phi}^0_h, \mathbf{\Phi}^1_h, \mathbf{\Phi}^2_h, \mathbf{\Phi}^3_h)$ and $(\mathbf{v}^b_h, \mathbf{\Psi}^0_h, \mathbf{\Psi}^1_h, \mathbf{\Psi}^2_h, \mathbf{\Psi}^3_h)$ in $\mathbf{V}^b_{\mathbf{h}} \times \mathbf{V}^0_{\mathbf{h^0}} \times \mathbf{V}^1_{\mathbf{h^1}} \times \mathbf{V}^2_{\mathbf{h^2}} \times \mathbf{V}^3_{\mathbf{h^3}}$,

$$\left| \begin{array}{rcl} \mathfrak{A}(\mathbf{u}^b_h, \mathbf{v}^b_h) & = & \displaystyle\int_{\Omega_b} \sigma(\mathbf{u}^b_h) : \overline{\varepsilon(\mathbf{v}^b_h)} - \widetilde{\rho}\omega^2 \mathbf{u}^b_h \cdot \overline{\mathbf{v}^b_h} - \sum_{j=0}^{3} i \int_{\Sigma^j_{bb}} \gamma^j \mathbf{u}^b_h \cdot \overline{\mathbf{v}^b_h}, \\ \mathfrak{B}^j_{\hat{\mathbf{h}}}(\mathbf{\Phi}^j_h, \mathbf{v}^b_h) & = & \displaystyle -\int_{\Sigma^j_{bb}} \Lambda^j_{\hat{\mathbf{h}}}(\mathbf{\Phi}^j_h) \cdot \overline{\mathbf{v}^b_h}, \quad j \in [\![0,3]\!], \\ \mathfrak{C}^j(\mathbf{u}^b_h, \mathbf{\Psi}^j_h) & = & \displaystyle -\int_{\Sigma^j_{aa}} \mathbf{u}^b_h \cdot \overline{\mathbf{\Psi}^j_h}, \quad j \in [\![0,3]\!], \\ \mathfrak{D}^{j\pm1}_{j,\hat{\mathbf{h}}}(\mathbf{\Phi}^{j\pm1}_h, \mathbf{\Psi}^j_h) & = & \displaystyle -\int_{\Sigma^j \cap \Omega^{j\pm1}} D^{j\pm1}_{j,\hat{\mathbf{h}}}(\mathbf{\Phi}^{j\pm1}_h) \cdot \overline{\mathbf{\Psi}^j_h}, \quad j \in \mathbb{Z}/4\mathbb{Z}. \end{array} \right. \tag{78}$$

If the meshes of the truncated lines $\Sigma^j_{\ell^j}$ are compatible with the mesh of Ω_b, in the sense that every segment of the mesh of $\Sigma^j_{\ell^j}$ is the edge of a triangle of the mesh of Ω_b and if the order of the elements is the same, $p = p^j$ for all j, a slighlty different version of the discrete HSM formulation is preferred. Indeed, in this case, one can reduce the number of degrees of freedom by enforcing the compatibility relation

$$\mathbf{\Phi}^j_h = \mathbf{u}^b_h \text{ on } \Sigma^j_{aa}, \quad j \in [\![0,3]\!],$$

at the discrete level. This leads to this second formulation:

Find $(\mathbf{u}_h^b, \mathbf{\Phi}_h^0, \mathbf{\Phi}_h^1, \mathbf{\Phi}_h^2, \mathbf{\Phi}_h^3) \in \mathbf{V}_{\mathbf{h}}^b \times \mathbf{V}_{\mathbf{h^0}}^0 \times \mathbf{V}_{\mathbf{h^1}}^1 \times \mathbf{V}_{\mathbf{h^2}}^2 \times \mathbf{V}_{\mathbf{h^3}}^3$ such that

$\mathbf{\Phi}_h^j = \mathbf{u}_h^b$ on $\Sigma_{aa}^j, j \in [\![0,3]\!]$, and such that $\forall (\mathbf{v}_h^b, \mathbf{\Psi}_h^0, \mathbf{\Psi}_h^1, \mathbf{\Psi}_h^2, \mathbf{\Psi}_h^3) \in \mathbf{V}_{\mathbf{h}}^b \times \mathbf{V}_{0,\mathbf{h^0}}^0 \times \mathbf{V}_{0,\mathbf{h^1}}^1 \times \mathbf{V}_{0,\mathbf{h^2}}^2 \times \mathbf{V}_{0,\mathbf{h^3}}^3$,

$$\left| \begin{array}{rcl} \mathfrak{A}(\mathbf{u}_h^b, \mathbf{v}_h^b) + \displaystyle\sum_{j=0}^{3} \mathfrak{B}_{\hat{\mathbf{h}}}^j(\mathbf{\Phi}_h^j, \mathbf{v}_h^b) & = & \displaystyle\int_{\partial\mathcal{O}} \sigma(\mathbf{u}^{inc}) \nu \cdot \overline{\mathbf{v}_h^b}, \\ \displaystyle\sum_{j=0}^{3} \left[\left(\int_{\Sigma^j} \mathbf{\Phi}_h^j \cdot \overline{\mathbf{\Psi}_h^j} \right) + \mathfrak{D}_{j,\hat{\mathbf{h}}}^{j-1}(\mathbf{\Phi}_h^{j-1}, \mathbf{\Psi}_h^j) + \mathfrak{D}_{j,\hat{\mathbf{h}}}^{j+1}(\mathbf{\Phi}_h^{j+1}, \mathbf{\Psi}_h^j) \right] & = & 0, \end{array} \right. \tag{79}$$

where $\mathbf{V}_{h,0}^j = \{\mathbf{\Psi}_h^j \in \mathbf{V}_h^j; \mathbf{\Psi}_h^j = 0 \text{ on } \Sigma_{aa}^j\}$ for $j \in [\![0,3]\!]$.

Even if the numerical method offers a great flexibility in the choice of the discretization parameters, in the numerical results in the sequel, we have chosen $p^j = p$, $h^j = h^0$ and $l^j = l^0$ for all j.

Remark 5.1. *Let us briefly comment the choice of the parameters a and b, and of the matrix γ^j which appears in the definition of the operators Λ^j (see (62) for the isotropic case and (74) for the anisotropic one). In practice, a is chosen as small as possible, the constraint being to satisfy (7). Then b is chosen slightly larger than a, in order to minimize the size of the 2D finite element domain Ω_b. Moreover, for γ^j we choose the approximation of the DtN maps in normal incidence. More precisely, using the notation of (74), γ^j is chosen such that $F^j(0) - i\gamma^j Q^j(0) = 0$. This leads to*

$$\gamma^j = \omega \begin{bmatrix} \sqrt{\rho(\lambda+2\mu)} & 0 \\ 0 & \sqrt{\rho\mu} \end{bmatrix} \quad \textit{and} \quad \gamma^j = \omega \begin{bmatrix} \sqrt{\rho C_{11}} & 0 \\ 0 & \sqrt{\rho C_{33}} \end{bmatrix}$$

in respectively the isotropic case and the orthotropic case. Note that this γ^j is the operator appearing in the first-order absorbing boundary conditions used in [55]. Let us mention that the choice of b and of γ^j may be more important when solving the problem with an iterative algorithm, using a sparse approximation as a preconditioner, in the spirit of [9]. In that case, as in domain decomposition methods [30], increasing the overlap $b - a$ and using for γ^j the approximation of the DtN map in normal incidence enable to speed up the convergence of iterative algorithms.

5.2. Numerical validation in the isotropic case

In the isotropic case, we can validate the HSM formulation comparing the results with an analytical solution in an homogeneous medium. We consider a pressure wave generated by a point source given by:

$$\mathbf{u}^{\text{ex}}(\mathbf{x}) = \frac{H'(k_P r)}{r} \begin{bmatrix} x \\ y \end{bmatrix}$$

where $r = \sqrt{x^2+y^2}$ and H is the Hankel function of the first kind. The function $\mathbf{u}^{ex}$ is of course the outgoing solution to

$$\left|\begin{array}{lll} -\mathrm{div}\,\sigma(\mathbf{u}) - \rho\omega^2\mathbf{u} = 0 & \text{in} & \Omega = \mathbb{R}^2 \setminus \mathcal{O}, \\ \mathbf{u} = \mathbf{u}^{\mathrm{ex}} & \text{on} & \partial\mathcal{O}, \end{array}\right. \tag{80}$$

for any obstacle $\mathcal{O} \subset \mathbb{R}^2$. The following results are obtained with a square obstacle $\mathcal{O} = [-0.2, 0, 2]^2$ and with the following material parameters and frequency:

$$\lambda = 16, \quad \mu = 2, \quad \rho = 1 \quad \text{and} \quad \omega = 20, \tag{81}$$

so that $k_P^2 = 20$ and $k_S^2 = 200$. For the discretization parameters, we use

$$\left|\begin{array}{l} (a, b) = (0.4, 0.5) \\ \mathbf{h} = (h, p) = (0.07, 2), \\ \mathbf{h^j} = (h^j, p^j, \ell^j) = (0.05, 2, 6) \;\; j \in [\![0, 3]\!], \\ \hat{\mathbf{h}} = (\hat{\ell}, \hat{h}, \hat{q}) = (30, 0.05, 10). \end{array}\right. \tag{82}$$

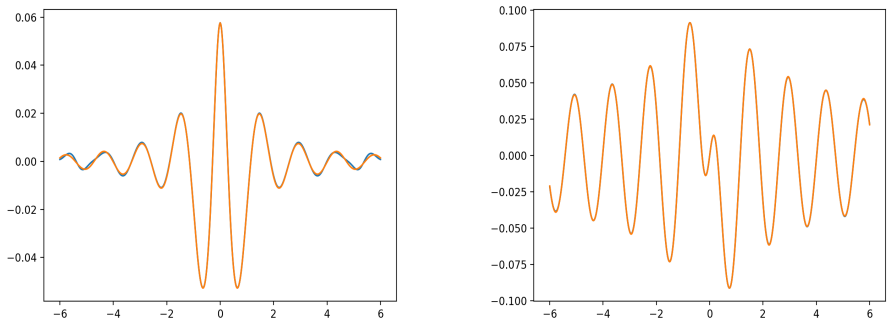

(a) $\mathbf{\Phi}_x^0$ (b) $\mathbf{\Phi}_y^0$

Figure 4: x component (a) and y component (b) of the trace of the computed solution (blue line) and the exact solution (orange line).

On Figure 4, we have represented the trace of the exact solution $\mathbf{\Phi}^0$ and of the approximated solution $\mathbf{\Phi}_h^0$ on the truncated line $\{x = a\} \times (-\ell^0, \ell^0)$. We can observe qualitatively a good agreement. In particular, the L^2-relative error $\frac{\|\mathbf{\Phi}^0 - \mathbf{\Phi}_h^0\|_2}{\|\mathbf{\Phi}^0\|_2}$ on the segment $\{x = a\} \times (-\ell^0, \ell^0)$ is around 0.011, and the L^2-relative error in Ω_b given by $\frac{\|\mathbf{u}^{\mathrm{ex}} - \mathbf{u}_h^b\|_2}{\|\mathbf{u}^{\mathrm{ex}}\|_2}$ is around 0.0029. We can observe that the $y-$ component of the trace of the solution is still not neglectable at the truncation distance $\ell^0 = 6$ (since u_y^{ex} decays as $\frac{1}{\sqrt{r}}$), but this does not seem to affect the accuracy of the approximation $\mathbf{u}_h^b$. This could be explained by the fact that even if we use an abrupt truncation of the traces, the half-space representations are valid up to infinity.

Since with the HSM method we compute (an approximation of) the trace $\mathbf{\Phi}^j$ on Σ^j and thanks to the analytical expressions of the solutions in the half-spaces Ω^j (see Lemma 4.3), we can reconstruct a posteriori (an approximation of) $\mathbf{u}^j$ in each half-space and then u in the whole domain. Note that different choices of reconstruction of $\mathbf{u}$ are possible (since the half-spaces Ω^j and Ω_b overlap). On Figure 5-(a), we have represented the solution using the identities

$$\mathbf{u} = \mathbf{U}^0(\mathbf{\Phi}^0) \text{ in } \Omega^0, \ \mathbf{u} = \mathbf{U}^1(\mathbf{\Phi}^1) \text{ in } \Omega^1 \setminus \Omega^0, \ \mathbf{u} = \mathbf{u}^b \text{ in } \Omega_b \setminus (\Omega^1 \cup \Omega^0).$$

As we can see, the different representations match at the various interfaces between the domains of representation, which illustrates the validity of the compatibility relations. On Figure 5-(b), we have represented the solution everywhere, the result being independent (up to a discretization error) of the choices of the representation in the overlapped areas. For comparison, we have represented the same reconstruction with a smaller $\hat{\ell}$. We have chosen $\hat{\ell} = 8$, so that $k_P < \hat{l} < k_S$, and as expected, the solution is no longer satisfactory. The good news is that, even if one does not know the exact solution, the discrepancy in the matching at the interfaces warns that the parameters have to be modified.

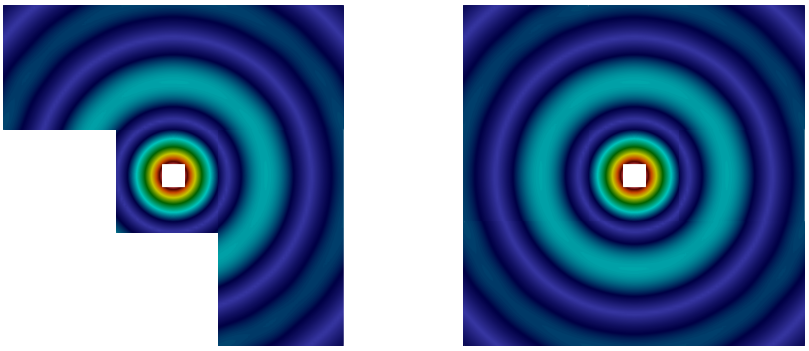

(a) The reconstructed solution in $\Omega^0 \cup \Omega^1 \cup \Omega_b$

(b) The reconstructed solution in Ω

Figure 5: Modulus of the reconstructed solution in $\Omega^0 \cup \Omega^1 \cup \Omega_b$ (a) and in Ω (b) using the discretization parameters (82).

Let us now study the influence of the various discretization parameters. First, we have represented on Figure 7 the L^2-relative error in Ω_b with respect to the mesh size h for two degrees of finite elements, $p = 1$ in blue and $p = 2$ in orange. As we can see, we recover the classical rate of convergence (2 for $p = 1$ and 3 for $p = 2$). We also see that for $p = 2$, a plateau is reached for the smallest values of h. This comes from the fact that the error due to the finite elements approximation becomes smaller than the error due to the truncation of the lines Σ^j. Indeed, by picking $\ell = 12$ instead of $\ell = 6$ and plotting the new error with respect to h with $p = 2$ (see the dotted line), the plateau moves down.

Now, let us study the effect of the parameters ℓ and $\hat{h}$. On Figure 8, we have represented the L^2-relative error in Ω_b with respect to ℓ for various values of $\hat{h} \in \{0.4, 0.2, 0.1, 0.05\}$.

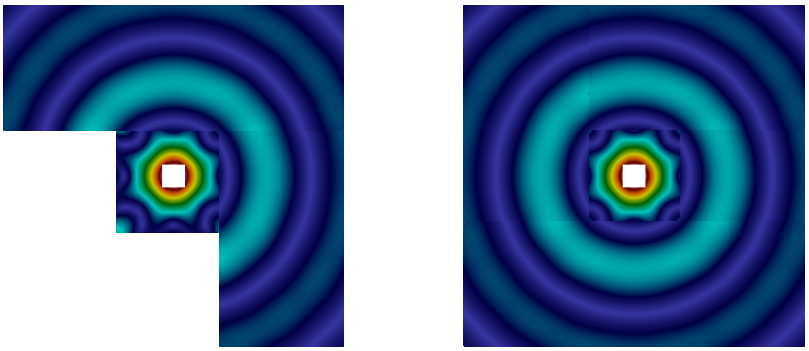

(a) The reconstructed solution in $\Omega^0 \cup \Omega^1 \cup \Omega_b$

(b) The reconstructed solution in Ω

Figure 6: Modulus of the reconstructed solution in $\Omega^0 \cup \Omega^1 \cup \Omega_b$ (a) and in Ω (b) using the discretization parameters (82) but with $\hat{l} = 8$.

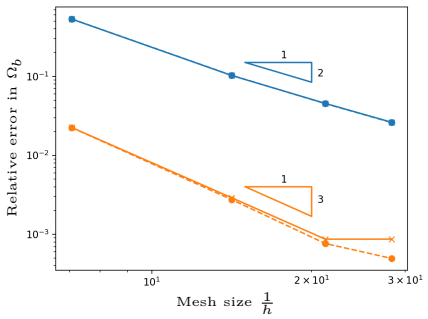

Figure 7: Relative error in Ω_b versus the mesh size h for $p = 1$ (in blue) and $p = 2$ (in orange). The continuous lines correspond to the case $\ell = 6$ and the dotted one to $\ell = 12$.

As we can see, the choice of $\hat{h}$ is related to the one of ℓ: if the parameter ℓ is chosen large, we must take $\hat{h}$ small enough to accurately compute the Fourier integral. In particular, the error decreases between $\ell = 12$ and $\ell = 24$ only in the case $\hat{h} = 0.05$. This means that only for sufficiently accurate quadrature formula the error will decrease with respect to the parameter ℓ. A first reason is the slow decay of the solution. Indeed by using the asymptotics of the Hankel function, we have

$$\mathbf{\Phi^0}(y) \underset{|y|\to+\infty}{\sim} \frac{1}{r^{\frac{3}{2}}} \begin{bmatrix} 0.4 \\ y \end{bmatrix} e^{ik_P r} \quad \text{where} \quad r = \sqrt{0.4^2 + y^2}.$$

This is responsible for the presence of peaks in the Fourier transform of the traces as represented on Figure 9 in blue for $\mathbf{\Phi}^0$ and in orange for $\mathbf{\Phi}_h^0$ computed with various values of ℓ. Note that as expected from the behavior of $\mathbf{\Phi^0}$, the peaks are stronger for the $y-$component. The larger ℓ is, the higher and thinner the

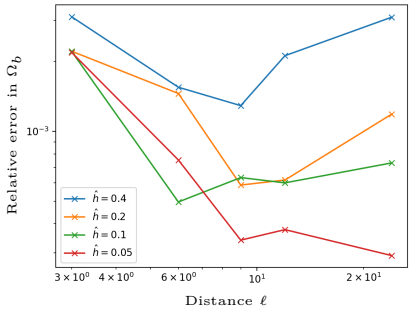

Figure 8: Relative error in Ω_b versus ℓ for different values of parameter $\hat{h}$

peaks are, which requires an adequate choice of the parameter $\hat{h}$.

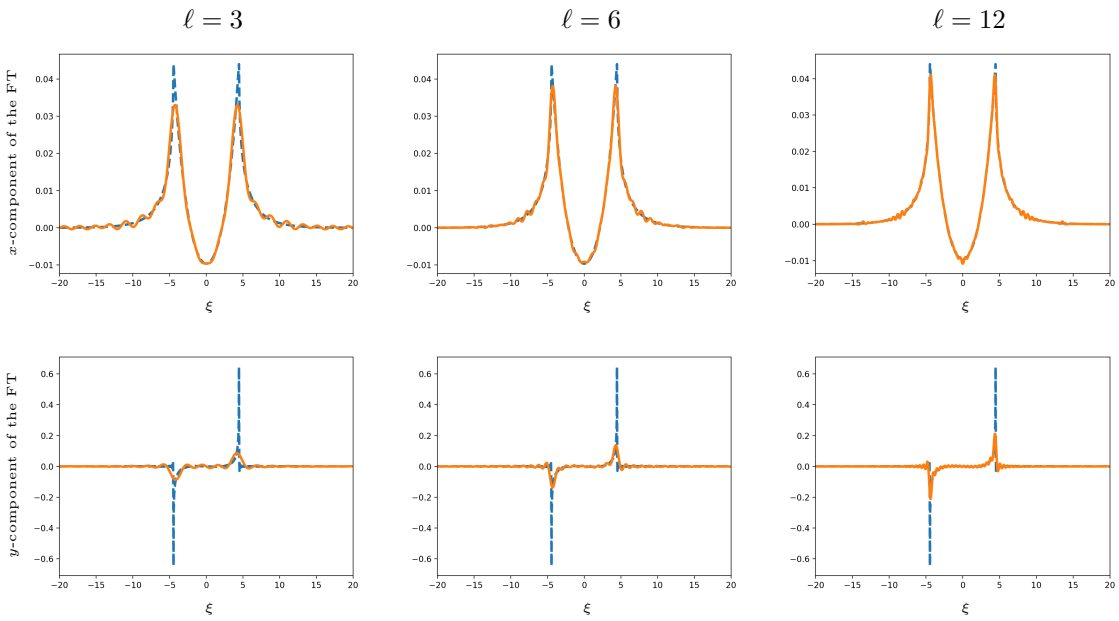

Figure 9: Real part of the Fourier transform of $\mathbf{\Phi^0}$ (dotted blue line) and $\mathbf{\Phi^0_h}$ (orange line) taking $\ell \in \{3, 6, 12\}$ (from left to right). On the top, we represent the x-component and, on the bottom, the y-component.

A second reason explaining the results of Figure 8 comes from the kernels appearing in the operators $D^j_{j\pm1}$ which oscillate more and more with respect to ξ for large values of x. To illustrate this point, we have represented on Figure 10 the integrand of D^0_1:

$$\frac{1}{\sqrt{2\pi}} Q(\xi) e^{i(K(\xi)(x-a)\pm\xi a)} Q^{-1}(\xi)\, \hat{\mathbf{\Phi}}(\xi) \tag{83}$$

for different values of x and taking $\mathbf{\Phi}$ as a 1D Lagrange basis function of order 1 (hat function) centered in $y = 0.5$ and with support in $[0.4, 0.6]$. We can also notice that the integrand becomes very small for $\xi \geq k_S$ ($\simeq 14$ in that case) since it is exponentially decaying. Solving the drawback of highly oscillating integrands by the use of asymptotic formulas will be the object of a forthcoming paper. Nevertheless, let us recall that, as we have seen, a small relative error can be achieved with reasonable discretization parameters.

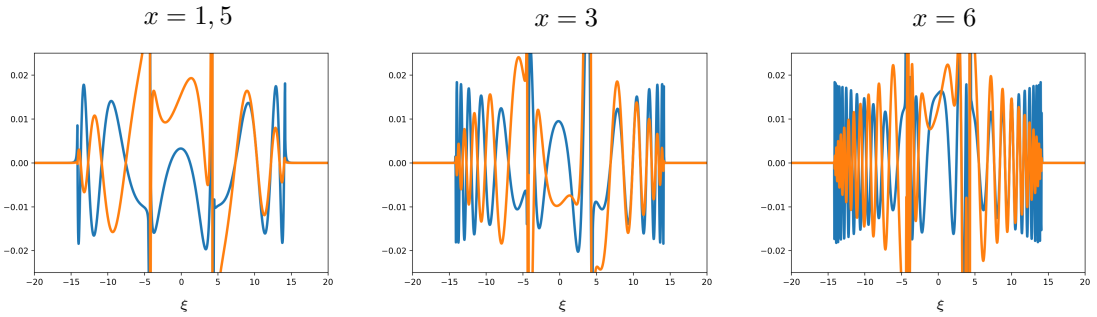

Figure 10: Real part of the x-component (in blue) and y-component (in orange) of the integrand term (83) versus ξ taking $x = \ell$.

5.3. Application to the diffraction problem in anisotropic media

Let us now show some numerical experiments for anisotropic media. We consider the diffraction of an incident Quasi-Shear plane wave. More precisely, we take

$$\mathbf{u}^{inc} = \mathbf{V}_1^0(\xi^{inc}) e^{i\kappa_1^0(\xi^{inc})x + i\xi^{inc}y}$$

where $\xi_{inc} < k_*$ and $|\kappa_1^0(\xi^{inc})| > |\kappa_2^0(\xi^{inc})|$, see Section 4.3.

The scatterer is a thin obstacle $\mathcal{O}$ which mimics a crack: it is the polygon delimited by the four points $(-0.2, -0.15)$, $(0, 0.01)$, $(0.12, 0.25)$ and $(0, 0)$. This problem fits into our initial problem (1) taking $\mathbf{f} = \mathbf{0}$ and $\mathbf{g} = -\sigma(\mathbf{u}^{inc})\nu$, the solution $\mathbf{u}$ being the diffracted field.

For these numerical simulations, we consider the four examples of homogeneous materials given in Section 1 characterized by their tensor $\widetilde{C} = C$ given in (26). We recall that the slowness diagrams associated to these materials are represented in Figure 1. In each case, we take $\widetilde{\rho} = \rho = 1$, $\omega = 20$ and $\xi_{inc} = 3$. For the discretization parameters, we use the same parameters (82) as for the isotropic validation case. On Figure 11, we have represented the (modulus of the) diffracted field $\mathbf{u}_h^b$ in Ω_b computed with the HSM method for the four materials. To test the "transparency" of the boundary condition on Σ_{bb}^j, we have computed the solution twice taking $b = 0.5$ and $b = 0.6$ and we have represented $u_{0.5}$ in $\Omega_{0.5}$ while $u_{0.6}$ is represented in $\Omega_{0.6} \setminus \Omega_{0.5}$ with a certain opacity. The two solutions match very well (up to a discretization error).

Again, since we compute an approximation of the trace $\mathbf{\Phi}^j$ on Σ^j and thanks to the analytical expression of the solution in the half-spaces Ω^j (see Lemma 4.8), we can reconstruct a posteriori (an approximation of)

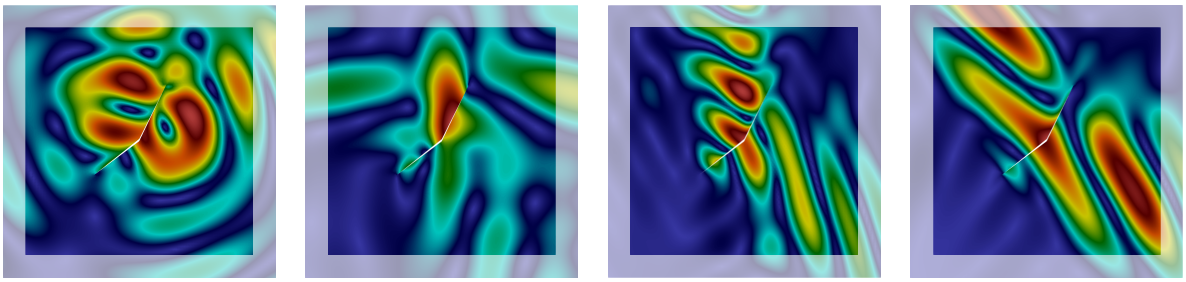

Figure 11: Modulus of the diffracted field $|\mathbf{u}_h^b| = \sqrt{\mathrm{Re}(u_x^b)^2 + \mathrm{Re}(u_y^b)^2}$.

$\mathbf{u}^j$ in the exterior domain. On Figure 12, we have represented the computed diffracted field $\mathbf{u}_h^b$ in Ω_b and the reconstructed fields $\mathbf{u}_h^j$ in Ω^j in the case of material **A**, the result being independent (up to a discretization error) of the choices of the representation in the overlapped areas.

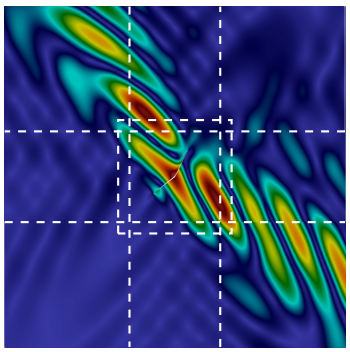

Figure 12: Modulus of the diffracted field in Ω considering material **A**.

The results presented in Figure 11 have shown that the computed solution is independent of the size of the square Ω_b. In the same spirit, the following test aims to check that the computed solution does not depend on the position of the infinite lines Σ^j of the HSM method. We compare two solutions, with the same material **O1** and the same source term, the only difference between them being a rotation of angle $\pi/3$ of the line Σ^j and the square Ω_b. As expected, one can observe a perfect matching between the two solutions, see Figure 13.

5.4. Comparison with the PML method for anisotropic media

In this section, we will compare the HSM method with the PML method. Let us briefly recall this last method. The idea is to apply a complex change of variable (this process is also called complex scaling of the cartesian coordinates) in a layer (denoted Ω_{PML}) surrounding the physical domain of interest (here Ω_b), see

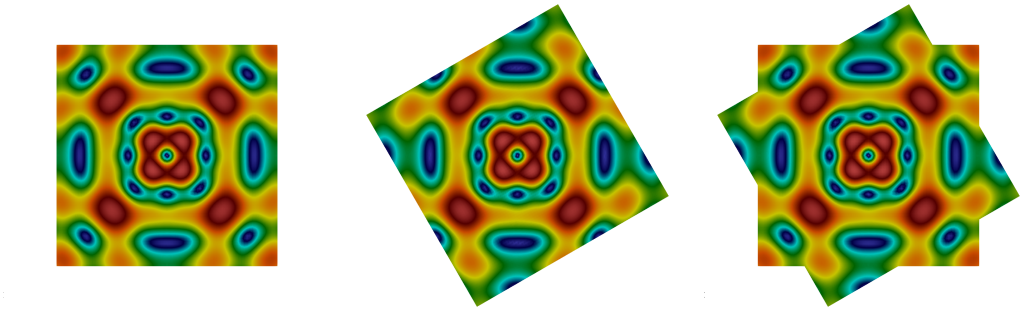

Figure 13: Modulus of the solution in Ω_b for two different orientations of the lines Σ^j and superposition of the two solutions.

Figure 14. The objective is that the layer "absorbs" the outgoing waves without producing any reflection at the interface between the physical domain and the layer. In the frequency domain, several changes of variable have been proposed in the literature (see for instance [20]) but the simplest one, that we use, is given by $\widetilde{x} := \zeta(x)$ and $\widetilde{y} := \zeta(y)$ where:

$$\zeta(t) = \alpha(t)(t-b)+b \ \text{ with } \ \alpha(t) = \begin{vmatrix} 1 & \text{if} & |t| < b, \\ \delta e^{i\theta} & \text{if} & |t| \geq b. \end{vmatrix} \tag{84}$$

Here $\delta > 0$ and $\theta \in]0, \frac{\pi}{2}[$ are two parameters of the PMLs. Another parameter is the thickness L of the PML layer Ω_{PML}. Then, we consider $\widetilde{\mathbf{u}}(\widetilde{x}, \widetilde{y})$ that satisfies the same partial differential equation than $\mathbf{u}$, replacing the derivatives with respect to (x, y) by the derivatives with respect to the stretched coordinates $(\widetilde{x}, \widetilde{y})$ (i.e. replacing the partial derivative ∂_x by $\partial_{\tilde{x}}$ and the partial derivative ∂_y by $\partial_{\tilde{y}}$). To get the PML formulation, we rewrite these equations in physical coordinates (x, y), which amounts to replace the partial derivative $\partial_{\tilde{x}}$ by $\frac{1}{\alpha(x)}\partial_x$ and the partial derivative $\partial_{\tilde{y}}$ by $\frac{1}{\alpha(y)}\partial_y$. Finally, at the boundary of the computational domain $\Omega_b \cup \Omega_{\text{PML}}$, one can impose homogeneous Dirichlet or Neumann boundary conditions.

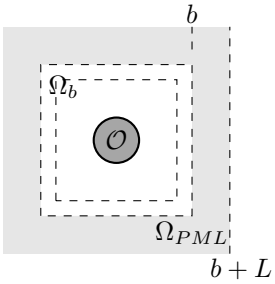

Figure 14: Description of the computational domain for the PML method.

In Figure 15, we have represented the results obtained by applying the PML method to the diffraction of

a shear or quasi-shear plane wave by the thin obstacle presented in Section 5.3. We have considered the four examples of homogeneous materials given in Section 3 whose tensors are given in (26), and with $\widetilde{\rho} = \rho = 1$, $\omega = 20$, $a = 0.4$ and $b = 0.5$. The PMLs parameters are $\delta = 4$, $L = 0.2$ (so that the computational domain is $[-0.7, 0.7]^2 \setminus \mathcal{O}$) and $\theta = \pi/3$ (first column), $\theta = \pi/4$ (second one) and $\theta = \pi/5$ (third one) and as before, we have used Lagrange finite elements of order 2. It seems that the method works well for the two first materials (in particular the isotropic one) whereas it is difficult to conclude for the two last ones. Let us now give some explanations.

First we focus on the isotropic material and explain why the PML method should work in this case. To simplify the explanations, let us consider for instance the half-space problem introduced in (37) for $j = 0$. We now apply the complex change of variable $x \to \zeta(x)$ while keeping the $y-$variable unchanged. We say that we have an infinite PML in the $x-$direction in Ω^0. We can understand the effect of this PML in this case, since we have a representation of the solution $\mathbf{U}^0$ before the change of variable, by Lemma 4.3. We deduce easily that after the change of variable, the obtained function writes as

$$\mathbf{U}_{\rm PML}(x,y) = \widetilde{\mathbf{U}}^0(\mathbf{\Phi})(\zeta(x),y) = \frac{1}{\sqrt{2\pi}} \int_{\mathbb{R}} Q(\xi) e^{i(K(\xi)(\zeta(x)-a)+\xi y)} [Q(\xi)]^{-1}(\xi)\, \hat{\mathbf{\Phi}}(\xi)\, d\xi, \quad x > a,\ y \in \mathbb{R}, \tag{85}$$

where $Q(\xi)$ is defined in (53) and $K(\xi)$ in (55). Here $\mathbf{U}_{\rm PML}$ is nothing else but the analytic continuation of $\mathbf{U}^0$ with respect to x on the line of the complex plane $x \to \zeta(x)$. In particular, by definition of ζ, $\mathbf{U}_{\rm PML} = \mathbf{U}^0$ in the "physical" layer $a < x < b$. This explains why the PML layer is said to be "perfectly matched" because it has no effect on the solution in the physical domain. Let us note that for each $x > a$, the matrix-valued function

$$\xi \to e^{i(K(\xi)(\zeta(x)-a)+\xi y)}$$

is still exponentially decaying since for $I \in \{P, S\}$, $\kappa_I(\xi)$ behaves like $i|\xi|$ for large $|\xi|$ and $\Re\big(\zeta(x) - a\big) > 0$ (since $\delta > 0$ and $\theta < \frac{\pi}{2}$). This implies that $\mathbf{U}_{\rm PML}$ is well-defined for $x > a$. Moreover, since we have also that for $I \in \{P, S\}$, $\kappa_I(\xi) \in \mathbb{R}^+$ for $|\xi| < k_I$ and $\Im\big(\zeta(x)\big) > 0$ for $x > b$ (since $\theta > 0$), the function $x \to \mathbf{U}_{\rm PML}(x, y)$ decays exponentially fast when x tends to infinity. This explains why the truncation of the PML in this case introduces only negligible reflections. By reproducing the same reasoning for PML layers in all directions, we understand why the PML method works for isotropic materials.

For anisotropic materials, one has to use the half-space representation U^j given in Lemma 4.8 and apply the same change of variable. Since for $I \in \{1, 2\}$ and $j \in \{0, 1, 2, 3\}$, $\Im(\kappa_I^j(\xi))$ is positive and behaves like $O(|\xi|)$, the integrand in ξ is exponentially decaying and the analytic continuation $\mathbf{U}^j_{\rm PML}$ is well-defined. But, what is not always true (and which can explain the numerical difficulties) is the decay of $\mathbf{U}^j_{\rm PML}$ with respect to x^j. This strongly depends on the anisotropy of the material.

For the orthotropic material **(O1)**, one has the same properties than in the isotropic case that is to say $\kappa_I^j(\xi)$ is either in $\mathbb{R}^+$ or in $i\mathbb{R}^+$, $I \in \{1, 2\}$ and $j \in \{0, 1, 2, 3\}$. In this case, $\mathbf{U}^j_{\rm PML}$ will decay exponentially

fast with respect to x^j and the PML method still works.

More generally, the PML method should work as soon as

$$\forall j \in \{0,1,2,3\},\ \forall I \in \{1,2\},\ \forall \xi \in \mathbb{R}, \quad \Im\left(e^{i\theta}\kappa_I^j(\xi)\right) > 0, \tag{86}$$

where for $I \in \{1,2\}$, $\kappa_I^j(\xi)$ is defined in Section 4.3. Unfortunately, this condition (86) is not always satisfied (see section 4.3):

- If there exist j, I, ξ s.t. $\kappa_I^j(\xi) \in \mathbb{R}^-$ (corresponding to *backward waves*), then the above condition can never be satisfied. This occurs for instance for material **(O2)** and **(A)**. In this case, $\mathbf{U}_{\mathrm{PML}}^j$ is exponentially growing, so the effect of truncation of the PML is not negligible anymore.

- An additional difficulty, which is less known, comes with the so-called *inhomogeneous waves*, i.e. there exist j and ranges of ξ for which $\kappa_I^j(\xi)$ is neither real nor purely imaginary (but is such that $\Im(\kappa_I^j(\xi)) > 0$ as required for an outgoing wave). In that case, there necessarily exists an inhomogeneous wave such that $\Re(\kappa_I^j(\xi)) < 0$. Indeed, by properties (65), either $\Re(\kappa_I^j(\xi)) < 0$ (and $\Im(\kappa_I^j(\xi)) > 0$) or $\Re(\kappa_I^j(-\xi)) < 0$ (and $\Im(\kappa_I^j(-\xi)) > 0$). Therefore, the condition (86) is not satisfied as soon as $\tan(\theta) > \Im(\kappa_I^j(\xi))/|\Re(\kappa_I^j(\xi))|$.

Very often, the two difficulties mentioned above occur together. In particular, one can show that inhomogeneous waves always exist if backward waves exist (for instance for materials **(O2)** and **(A)**). The converse is not true, and one can exhibit anisotropic materials for which inhomogeneous waves exist without backward waves, as for material **(O3)** (see also material V in [14]). In that case, the PMLs should work for a parameter θ small enough if

$$\inf_{\xi\in\mathbb{R}} \frac{\Im(\kappa_I^j(\xi))}{|\Re(\kappa_I^j(\xi))|} > 0, \quad j \in \{0,1,2,3\},\ \ I \in \{1,2\}.$$

Does it definitely mean that for a material which generates backward waves or inhomogeneous waves, PMLs do not work ? Let us mention that in the time-domain regime, the presence of backward waves in the x-direction, responsible of an exponential behavior of the PML solution, results in strong instabilities of the PMLs as explained in [14]. On the other hand, the presence of inhomogeneous waves results in long-time instabilities (see [14, 6, 17]). For the frequency-domain regime, the situation is not so clear, since as mentioned in the introduction of this paper, PMLs may work for some models for which they are unstable in the time-domain. We will observe how the PMLs behave on some numerical illustrations.

We come back to the numerical results in Figure 15. As we have noticed previously, PMLs work well for the isotropic material **ISO** as well as for material **(O1)**, which both do not generate any backward nor inhomogeneous waves : they give similar results to the HSM method, whatever the angle θ. Concerning the two last anisotropic materials **(O2)** and **(A)**, which generate both backward and inhomogeneous waves,

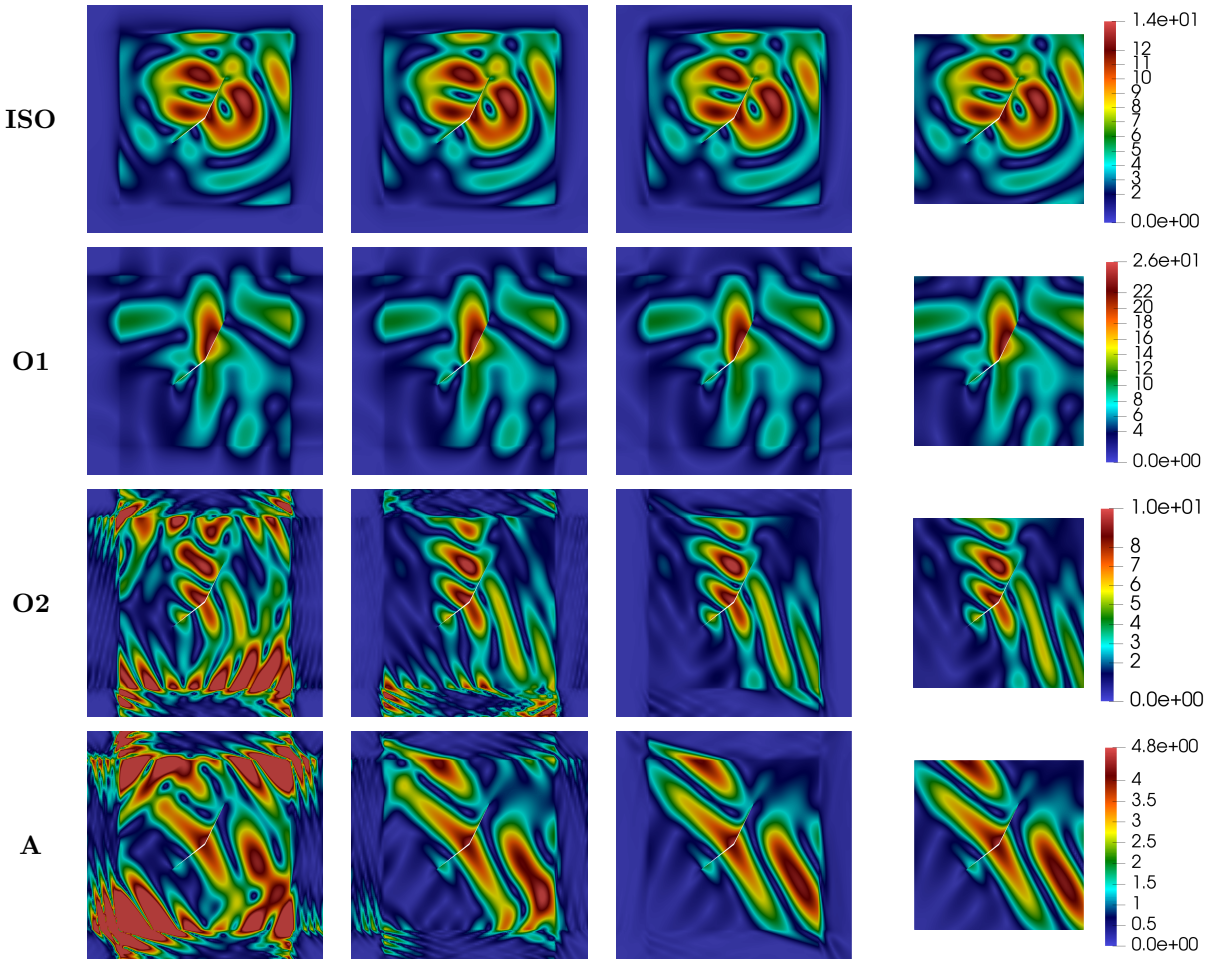

Figure 15: Modulus of the diffracted field $|\mathbf{u}_h^b| = \sqrt{\Re(u_x^b)^2 + \Re(u_y^b)^2}$ computed using PML method (first three columns) with $L = 0.2$ and for various values of $\theta = \{\frac{\pi}{3}, \frac{\pi}{4}, \frac{\pi}{5}\}$ (from left to right). The results obtained with the HSM method are recalled in the last column.

we observe perturbations of the solution for the angles $\theta = \frac{\pi}{3}$ and $\theta = \frac{\pi}{4}$ but they seem to disappear when decreasing the angle to $\theta = \frac{\pi}{5}$ and the results again look similar to the ones obtained with the HSM method. To assess the PMLs with $\theta = \frac{\pi}{5}$, we have computed the difference between the solutions in the physical regions $[-b, b]^2 \setminus \mathcal{O}$ using the PML method and the HSM method, for the isotropic medium **ISO** and the anisotropic medium **(A)**. This difference is presented in Figure 16 for three different sizes of the PMLs, $L = 0.2$, 0.3 and 0.5. In the isotropic case, we can observe that the difference reduces as L grows, up to the discretization error of the two methods. This can be explained by the fact that, for a large enough layer, the truncation of the PMLs do not have anymore impact on the solution. On the contrary, in the anisotropic case, the error does not decrease when the size of the PMLs grows, it even increases, which shows that the PML solution does not converge as the length of the layer grows. This non convergence can be explained

by the fact that this time $\mathbf{U}_{\mathrm{PML}}$ is exponentially growing inside the layers due to presence of backward and inhomogeneous waves.

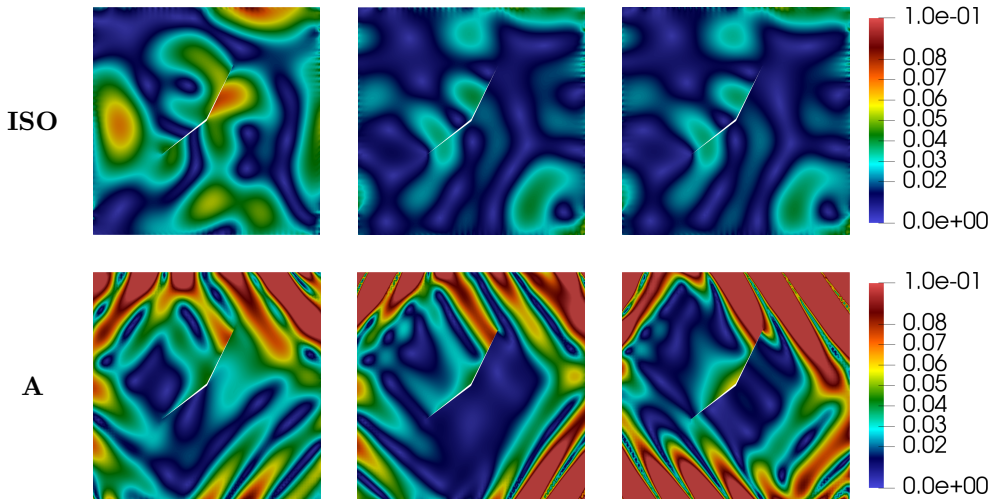

Figure 16: Modulus of the difference between the PML ($\theta = \pi/5$) and HSM solutions in Ω_b for different sizes of layers $L = \{0.2, 0.3, 0.5\}$. On the first line, the isotropic medium, and on the bottom line the anisotropic medium. The color scale is the same for all images.

Finally, let us present a last case, an orthotropic medium with no inverse waves but with inhomogeneous waves. We consider the material defined by

$$\textbf{(O3)} \quad C = \begin{bmatrix} 18 & 8 & 0 \\ 8 & 21 & 0 \\ 0 & 0 & 7 \end{bmatrix}. \tag{87}$$

The corresponding slowness diagram is given in Figure 17. We have also represented in this figure the position in the complex plane of $\kappa_1^0(\xi)$ and $\kappa_2^0(\xi)$ for $\xi \in [-50, 50]$ and $\omega = 90$.

For this last material, we have considered the same diffraction problem as before but with a larger frequency $\omega = 90$. In Figure 18, we give the results obtained using the PML method taking $\theta = \frac{\pi}{2.5}$, $\frac{\pi}{3}$ and $\frac{\pi}{4}$. We have also represented in the complex plane the position of $e^{i\theta}\kappa_1^0(\xi)$ and $e^{i\theta}\kappa_2^0(\xi)$ for $\xi \in [-50, 50]$. As we can see, the condition (86) is satisfied for $\theta = \frac{\pi}{4}$ and $\frac{\pi}{3}$, but is not satisfied for $\theta = \frac{\pi}{2.5}$. For $\theta = \frac{\pi}{3}$ and $\frac{\pi}{4}$, the results obtained with PML and HSM are very similar. For $\theta = \frac{\pi}{2.5}$, the PML solution is in particular wrong near the PML interface and the obstacle (see left bottom corner).

In conclusion, for anisotropic materials, as soon as there is the presence of inhomogeneous waves, one has to be really careful for chosing the PMLs parameters: PMLs could work with some specific choices of the parameters but this is in general not obvious to determine them in advance and they have to be adapted

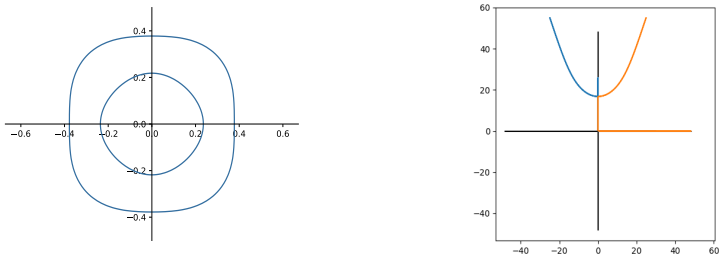

(O3)

Figure 17: Slowness diagram of the orthotropic material **O3** (on the left) and position of the wave number $\kappa_1^0(\xi)$ (in blue) and $\kappa_2^0(\xi)$ (in orange) in the complex plane (on the right).

to the material and to the frequency. Therefore, there is a clear lack of robustness of the PML method in this case.

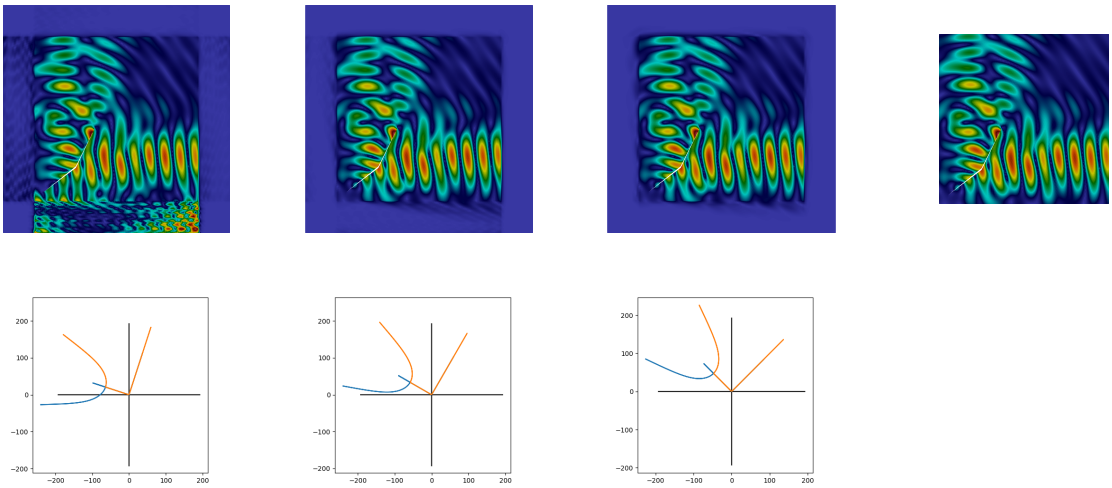

Figure 18: Modulus of the diffracted field computed using PML method (first three columns) for $\theta = \frac{\pi}{2.5}, \frac{\pi}{3}$ and $\frac{\pi}{4}$ (from left to right) and using HSM method (last column). On the second line, position of $e^{i\theta}\kappa_1^0(\xi)$ (in blue) and $e^{i\theta}\kappa_2^0(\xi)$ (in orange) in the complex plane.

6. Conclusions and ongoing works

In this paper we have presented a new numerical method to solve scattering problems with unbounded anisotropic elastic backgrounds. The method has been validated through several numerical results in both isotropic and anisotropic media. There is still work to be done in the future. As mentioned in Section 4.1,

we need to find an adequate framework to establish the well-posedness of the HSM formulation. This is a preliminary step for proving convergence results as it was done for the scalar dissipative case in [26].

Besides, a practical question concerns the computation of oscillating Fourier integrals (see section 5.2): some solutions are currently investigated for the scalar case using the stationary phase theorem or deforming the Fourier path in the complex plane.

The HSM method provides reference solutions which can be compared to the solutions obtained with classical cartesian PMLs. This allows to check the validity of the PMLs, in particular in situations where they are known to be unstable in the time-domain. The conclusion is that in absence of backward waves in the PMLs' directions, we can always choose the parameters so that the PMLs work. Note that this choice, which depends only on the background, can be very constrained in presence of inhomogeneous waves. In presence of backward waves, the PMLs do not work in general, with results deteriorating all the more as the dissipation of the PML increases. A prospect is to better understand and justify these observations theoretically.

Finally let us mention the possibility of combining the ideas of both the HSM and the PML methods, introducing the so-called "complex-scaled traces", as it was done for the Helmholtz equation in [25]. A main advantage of this "complex-scaled HSM" method is to recover exponentially decaying traces like in the dissipative case.

Appendix A. Energy flux and limiting absorption principle

The inequality (30) can be established using a limiting absorption technique. The idea is to add to the frequency ω a small imaginary part: $\omega_\varepsilon = \omega + i\varepsilon$ with $\varepsilon > 0$. Then outgoing plane waves become exponentially decaying and the result can be obtained by simple integration by part. More precisely, suppose $\mathcal{F}(k_x, k_y, \omega) = 0$, $\partial_\omega \mathcal{F}(k_x, k_y, \omega) \neq 0$ and $\mathbf{v}_g(\mathbf{k}) \cdot \mathbf{e}_x \neq 0$. We deduce by (28) that $\partial_{k_x} \mathcal{F}(k_x, k_y, \omega) \neq 0$. Then, by the implicit function theorem, for $\varepsilon > 0$ small enough, there exists $k_x^\varepsilon \in \mathbb{C}$ such that $\mathcal{F}(k_x^\varepsilon, k_y, \omega_\varepsilon) = 0$. Differentiating this identity with respect to ε and using again (28) leads to

$$\frac{k_x^\varepsilon - k_x}{\varepsilon} \to i\mathbf{v}_g(\mathbf{k}) \cdot \mathbf{e}_x. \tag{A.1}$$

Let us define the associated plane wave $\mathbf{u}_\varepsilon(x, y) = \mathbf{U}_\varepsilon e^{i(k_x^\varepsilon x + k_y y)}$ where $\mathbf{U}_\varepsilon \in \mathbb{C}^2$ satisfies $\mathcal{A}(k_x^\varepsilon . k_y)\mathbf{U}_\varepsilon = \omega_\varepsilon^2 \mathbf{U}_\varepsilon$ and $|\mathbf{U}_\varepsilon| = 1$. Since $\mathbf{v}_g(\mathbf{k}) \cdot \mathbf{e}_x > 0$ which implies $\Im(k_x^\varepsilon) > 0$, $\mathbf{u}_\varepsilon$ is exponentially decaying in x. One can then write:

$$\int_0^{+\infty} \left[\sigma(\mathbf{u}_\varepsilon) : \varepsilon(\bar{\mathbf{u}}_\varepsilon) - \omega_\varepsilon^2 |\mathbf{u}_\varepsilon|^2\right] dx = -[\sigma(\mathbf{u}_\varepsilon)\mathbf{e}_x \cdot \bar{\mathbf{u}}_\varepsilon]_{|x=0}$$

where all terms of the previous identity are independent of y. Taking the imaginary part gives

$$\Im[\sigma(\mathbf{u}_\varepsilon)\mathbf{e}_x \cdot \bar{\mathbf{u}}_\varepsilon]_{|x=0} = \frac{\omega\varepsilon}{\Im(k_x^\varepsilon)}$$

which, by (A.1), tends to $\omega/(\mathbf{v}_g(\mathbf{k}) \cdot \mathbf{e}_x)$ when $\varepsilon \to 0$.

Appendix B. The roots of P_ξ are simple, except for discrete values of ξ

Let us prove this result by contradiction and suppose that P_ξ has a root $\kappa(\xi)$ of multiplicity 2 for all $\xi \in I$ where $I \subset \mathbb{R}$ is some non empty interval. From the results of section 3, we know that this can occur only if $\forall \xi \in I$, $\kappa(\xi) \notin \mathbb{R}$. But then $\overline{\kappa(\xi)}$ is also a root of P_ξ of multiplicity 2, for all $\xi \in I$. Summing up, P_ξ must have the following form for $\xi \in I$:

$$P_\xi(\kappa) = A_0 \left[(\kappa - \kappa(\xi))(\kappa - \overline{\kappa(\xi)})\right]^2$$

which can be rewritten as follows:

$$P_\xi(\kappa) = A_0 \left[\kappa^2 - 2a(\xi)\kappa + \rho(\xi)\right]^2 \tag{B.1}$$

where $a(\xi) = \Re(\kappa(\xi))$ and $\rho(\xi) = |\kappa(\xi)|^2$. On the other hand, from the definition $P_\xi(\kappa) = \mathcal{F}(\kappa, \xi, \omega)$ where $\mathcal{F}$ is defined by (50), we know that for all $\xi \in \mathbb{R}$,

$$P_\xi(\kappa) = \sum_{j=0}^{4} A_{4-j}(\xi)\kappa^j \tag{B.2}$$

where $A_0(\xi) = A_0$ and $A_j(\xi)$ is a polynomial function of ξ of degree j. By identification between (B.1) and (B.2), we deduce that for all $\xi \in I$,

$$-4A_0\, a(\xi) = A_1(\xi) \tag{B.3}$$

$$2A_0(\rho(\xi) + 2a(\xi)^2) = A_2(\xi) \tag{B.4}$$

$$-4A_0\, a(\xi)\rho(\xi) = A_3(\xi) \tag{B.5}$$

$$A_0\rho(\xi)^2 = A_4(\xi) \tag{B.6}$$

Equation (B.3) shows that $a(\xi)$ is a polynomial function of ξ, and then also $\rho(\xi)$ by equation (B.4). Thus the functions $a(\xi)$ and $\rho(\xi)$ which were a priori defined only for $\xi \in I$ can be extended to all $\xi \in \mathbb{R}$, and the identities (B.3) to (B.6) are in fact valid for all $\xi \in \mathbb{R}$. This is equivalent to say that identity (B.1) is valid for all $\xi \in \mathbb{R}$. But then P_ξ would have two roots of multiplicity 2 for all $\xi \in \mathbb{R}$, which is not the case as explained in section 3.

Appendix C. $\mathbf{V}_1^0(\xi)$ and $\mathbf{V}_2^0(\xi)$ are linearly independent

Let, for a fixed $\xi \in \mathbb{R}$, denote by κ_1 and κ_2 the two roots of P_ξ corresponding to outgoing waves, as explained in section 4.3, and let $\mathbf{V}_1$ and $\mathbf{V}_2$ be two corresponding eigenvectors. We want to show by contradiction that $\mathbf{V}_1$ and $\mathbf{V}_2$ are linearly independent. If not, it means that there exists a non-zero vector $\mathbf{U} \in \mathbb{C}^2$ such that $\mathcal{A}(\kappa_1, \xi)\mathbf{U} = \omega^2\mathbf{U}$ and $\mathcal{A}(\kappa_2, \xi)\mathbf{U} = \omega^2\mathbf{U}$, where we recall that

$$\mathcal{A}(\kappa, \xi) = \frac{1}{\rho}[\kappa^2\mathcal{A}_0 + \kappa\xi(\mathcal{A}_1 + \mathcal{A}_1^{\mathrm{T}}) + \xi^2\mathcal{A}_2],$$

the matrices $\mathcal{A}_j$ being defined by (15). Then, projecting these two equations on $\mathbf{U}$, we deduce that κ_1 and κ_2 are the two roots of the equation

$$(\overline{\mathbf{U}}^{\mathrm{T}}\mathcal{A}_0\mathbf{U})\kappa^2 + (\overline{\mathbf{U}}^{\mathrm{T}}(\mathcal{A}_1+\mathcal{A}_1^{\mathrm{T}})\mathbf{U})\kappa\xi + (\overline{\mathbf{U}}^{\mathrm{T}}\mathcal{A}_2\mathbf{U})\xi^2 - (\overline{\mathbf{U}}^{\mathrm{T}}\mathbf{U})\omega^2\rho = 0 \tag{C.1}$$

Note that, since the matrices $\mathcal{A}_0$, $\mathcal{A}_2$ and $(\mathcal{A}_1+\mathcal{A}_1^{\mathrm{T}})$, are real and symmetric, the equation (C.1) has real coefficients. A direct consequence is that κ_1 and κ_2 must be real. Indeed, if for instance $\kappa_1 \notin \mathbb{R}$, then necessarily $\kappa_2 = \overline{\kappa_1}$, but this is impossible since complex roots corresponding to outgoing waves have a positive imaginary part (see section 4.3).

Now let us set for $m = 1, 2$, $\mathbf{U}^{(m)}(x, y) = \mathbf{U}e^{i(\kappa_m(x-a)+\xi y)}$. Then, according to the selection of outgoing waves, we must have $\Im(\sigma(\mathbf{U}^{(m)})\mathbf{e}_x \cdot \overline{\mathbf{U}^{(m)}}) > 0$ for $m = 1, 2$ which can be rewritten as follows (see (29)):

$$(\overline{\mathbf{U}}^{\mathrm{T}}\mathcal{A}_0\mathbf{U})\kappa_m + (\overline{\mathbf{U}}^{\mathrm{T}}(\mathcal{A}_1+\mathcal{A}_1^{\mathrm{T}})\mathbf{U})\frac{\xi}{2} > 0, \quad m = 1, 2. \tag{C.2}$$

From (C.1) and (C.2), we deduce that each root κ_m is locally a holomorphic function of ω, such that:

$$\frac{d\kappa_m}{d\omega}(\omega) = \left((\overline{\mathbf{U}}^{\mathrm{T}}\mathcal{A}_0\mathbf{U})\kappa_m + (\overline{\mathbf{U}}^{\mathrm{T}}(\mathcal{A}_1+\mathcal{A}_1^{\mathrm{T}})\mathbf{U})\frac{\xi}{2}\right)^{-1}(\overline{\mathbf{U}}^{\mathrm{T}}\mathbf{U})\,\omega\rho > 0.$$

Using again (C.2), this implies that for $\varepsilon > 0$ small enough, setting $\kappa_m^\varepsilon = \kappa_m(\omega + i\varepsilon)$, we have $\Im(\kappa_m^\varepsilon) > 0$, $m = 1, 2$, which is false: indeed one has for instance $\kappa_1^\varepsilon + \kappa_2^\varepsilon \in \mathbb{R}$ since

$$\kappa_1^\varepsilon + \kappa_2^\varepsilon = -\frac{\overline{\mathbf{U}}^{\mathrm{T}}(\mathcal{A}_1+\mathcal{A}_1^{\mathrm{T}})\mathbf{U}}{\overline{\mathbf{U}}^{\mathrm{T}}\mathcal{A}_0\mathbf{U}}\xi.$$

Appendix D. Formulas for the normal stress of the half-space representation in the anisotropic case

Let us derive the expression of the matrices $F^j(\xi)$ which appear in the the expression of the operators Λ^j. In the general case, we need to consider separately each half-space. As in Section 4.2, the operators Λ^j are given by (61) where the fields $\mathbf{T}^j(\mathbf{\Phi})$, for $j = 0, 1, 2, 3$ are defined in (59). Using (14), we get the following expressions.

- For $j = 0$, we have for $x_0 > a$, $y_0 \in \mathbb{R}$

$$\mathbf{T}^0(\mathbf{\Phi})(x_0, y_0) = \mathcal{A}_0\partial_{x_0}\mathbf{U}^0(\mathbf{\Phi})(x_0, y_0) + \mathcal{A}_1\partial_{y_0}\mathbf{U}^0(\mathbf{\Phi})(x_0, y_0).$$

  Using (69), we deduce that for $x_0 > a$, $y_0 \in \mathbb{R}$

$$\mathbf{T}^0(\mathbf{\Phi})(x_0, y_0) = \frac{1}{\sqrt{2\pi}}\int_{\mathbb{R}} F^0(\xi)e^{i(K^0(\xi)(x_0-a)+\xi y_0)}Q^0(\xi)^{-1}\,\hat{\mathbf{\Phi}}(\xi)\,d\xi, \tag{D.1}$$

  where $Q^0(\xi)$ is defined in (68), $K^0(\xi)$ in (70) and $F^0(\xi)$ is given by

$$F^0(\xi) := i\mathcal{A}_0Q^0(\xi)K^0(\xi) + i\xi\mathcal{A}_1Q^0(\xi).$$

- In the same way, for $j = 1$, we have for $x_1 > a$, $y_1 \in \mathbb{R}$

$$\mathbf{T}^1(\mathbf{\Phi})(x_1, y_1) = \frac{1}{\sqrt{2\pi}} \int_{\mathbb{R}} F^1(\xi) e^{i(K^1(\xi)(x_1-a)+\xi y_1)} Q^1(\xi)^{-1} \mathcal{R}(\theta_1) \hat{\mathbf{\Phi}}(\xi)\, d\xi \tag{D.2}$$

where $Q^1(\xi)$ and $K^1(\xi)$ are defined in (71) and $F^1(\xi)$ is given by

$$F^1(\xi) := i\mathcal{A}_1^T Q^1(\xi) K^1(\xi) - i\xi \mathcal{A}_2 Q^1(\xi).$$

- For $j = 2$, we have for $x_2 > a$, $y_2 \in \mathbb{R}$

$$\mathbf{T}^2(\mathbf{\Phi})(x_2, y_2) = \frac{1}{\sqrt{2\pi}} \int_{\mathbb{R}} F^2(\xi) e^{i(K^2(\xi)(x_2-a)+\xi y_2)} Q^2(\xi)^{-1} \mathcal{R}(\theta_2) \hat{\mathbf{\Phi}}(\xi)\, d\xi, \tag{D.3}$$

where $Q^2(\xi)$ and $K^2(\xi)$ are defined in (71) and $F^2(\xi)$ is given by

$$F^2(\xi) := i\mathcal{A}_0 Q^2(\xi) K^2(\xi) + i\xi \mathcal{A}_1 Q^2(\xi).$$

- Finally, for $j = 3$, we have for $x_1 > a$, $y_1 \in \mathbb{R}$

$$\mathbf{T}^3(\mathbf{\Phi})(x_3, y_3) = \frac{1}{\sqrt{2\pi}} \int_{\mathbb{R}} F^3(\xi) e^{i(K^3(\xi)(x_3-a)+\xi y_3)} Q^3(\xi)^{-1} \mathcal{R}(\theta_3) \hat{\mathbf{\Phi}}(\xi)\, d\xi \tag{D.4}$$

where $Q^3(\xi)$ and $K^3(\xi)$ are defined in (71) and $F^3(\xi)$ is given by

$$F^3(\xi) := i\mathcal{A}_2 Q^3(\xi) K^1(\xi) - i\xi \mathcal{A}_1^{\mathrm{T}} Q^3(\xi).$$

References

[1] S. Abarbanel and D. Gottlieb. A mathematical analysis of the PML method. *J. Comput. Phys*, 134(2):357–363, 1997.

[2] S. Abarbanel, D. Gottlieb, and J.S. Hesthaven. Long Time Behavior of the Perfectly Matched Layer Equations in Computational Elactromagnetics. *J. Scientific Comp.*, 17(1-4):405–422, 2002.

[3] C. Alves and T. Ha Duong. Numerical resolution of the boundary integral equations for elastic scattering by a plane crack. *Int. J. Numer. Methods Eng.*, 38(14):2347–2371, 1995.

[4] D. Ang, , I. Masaru Ikehata, D. Trong, and M. Yamamoto. Unique continuation for a stationary isotropic lamé system with variable coefficients. pages 599–617.

[5] D. Appelö, T. Hagstrom, and G. Kreiss. Perfectly matched layers for hyperbolic systems: General formulation, well-posedness, and stability. *SIAM J. Appl. Math.*, 67(1):1–23, 2006.

[6] D. Appelö and G. Kreiss. A new absorbing layer for elastic waves. *J. Comput. Phys.*, 215(2):642–660, 2006.

[7] D. H. Baffet, M. J. Grote, S. Imperiale, and M. Kachanovska. Energy Decay and Stability of a Perfectly Matched Layer For the Wave Equation. *J. Sci. Comput.*, November 2019.

[8] N. S. Bakhvalov and G. Panasenko. *Homogenisation: averaging processes in periodic media: mathematical problems in the mechanics of composite materials*, volume 36. Springer Science & Business Media, 2012.

[9] V. Baronian, A-S. Bonnet-Ben Dhia, S. Fliss, and A. Tonnoir. Iterative methods for scattering problems in isotropic or anisotropic elastic waveguides. *Wave Motion*, 64:13–33, 2016.

[10] H. Barucq, L. Boillot, H. Calandra, and J. Diaz. Absorbing boundary conditions for 2D tilted transverse isotropic elastic media. In *Congrès SMAI 2013*, volume 45 of *ESAIM Proc. Surveys*, pages 400–409. EDP Sci., Les Ulis, 2014.

[11] U. Basu and A. K. Chopra. Perfectly matched layers for transient elastodynamics of unbounded domains. *Int. J. Numer. Methods Eng.*, 59(8):1039–1074, 2004.

[12] A. Bayliss and E. Turkel. Radiation boundary conditions for wave-like equations. *Comm. Pure and Applied Math.*, 33(6):707–725, 1980.

[13] E. Bécache, A.-S. Bonnet-BenDhia, and G. Legendre. Perfectly matched layers for the convected helmholtz equation. *SIAM J. Numer. Anal.*, 42:409–433, 2004.

[14] E. Bécache, S. Fauqueux, and P. Joly. Stability of perfectly matched layers, group velocities and anisotropic waves. *J. Comput. Phys.*, 188(2):399–433, 2003.

[15] E. Bécache, D. Givoli, and T. Hagstrom. High-order Absorbing Boundary Conditions for anisotropic and convective wave equations. *J. Comput. Phys.*, 229(4):1099–1129, 2010.

[16] E. Bécache and P. Joly. On the analysis of Bérenger's perfectly matched layers for Maxwell's equations. *ESAIM: Mathematical Modelling and Numerical Analysis*, 36(1):87–119, January 2002.

[17] E. Bécache, P. G. Petropoulos, and S. D. Gedney. On the long-time behavior of unsplit perfectly matched layers. *IEEE Trans. Antennas Propag.*, 52(5):1335–1342, 2004.

[18] J.-P. Bérenger. A perfectly matched layer for the absorption of electromagnetic waves. *J. Comput. Phys.*, 114(2):185–200, 1994.

[19] A. Bermudez, L. Hervella-Nieto, A. Prieto, and R. Rodriguez. An exact bounded pml for the helmholtz equation. *C. R. Math.*, 339(11):803–808, 2004.

[20] A. Bermudez, L. Hervella-Nieto, A. Prieto, and R. Rodrıguez. An optimal perfectly matched layer with unbounded absorbing function for time-harmonic acoustic scattering problems. *J. Comput. Phys.*, 223(2):469–488, 2007.

[21] M. Bonnet. *Boundary integral equations methods in solids and fluids*. John Wiley and sons, 1999.

[22] M. Bonnet. Solvability of a volume integral equation formulation for anisotropic elastodynamic scattering. *J. Integral Equations Appl.*, 28(2):169–203, 2016.

[23] A.-S. Bonnet-Ben Dhia, C. Chambeyron, and G. Legendre. On the use of perfectly matched layers in the presence of long or backward propagating guided elastic waves. *Wave Motion*, 51(2):266–283, 2014.

[24] A.-S. Bonnet-BenDhia, S. Chandler-Wilde, and S. Fliss. On the half-space matching method for real wavenumbers. *SIAM J. Appl. Math.*, 82(4), 2022.

[25] A.-S. Bonnet-BenDhia, S. Chandler-Wilde, S. Fliss, C. Hazard, Karl-Michael Perfekt, and Y. Tjandrawidjaja. The complex-scaled half-space matching method. *SIAM J. Math. Anal.*, 54:512–557, 1 2022.

[26] A-S. Bonnet-BenDhia, S. Fliss, and Y. Tjandrawidjaja. *Numerical analysis of the Half-Space Matching method with Robin traces on a convex polygonal scatterer*, pages 105–144. Maxwell's Equations: Analysis and Numerics, 5 2019.

[27] J. H. Bramble and J. E. Pasciak. Analysis of a finite pml approximation for the three dimensional time-harmonic maxwell and acoustic scattering problems. *Math. Comput.*, pages 597–614, 2006.

[28] J. H. Bramble and J. E. Pasciak. Analysis of a cartesian pml approximation to acoustic scattering problems in r2 and r3. *J. Comput. Appl. Math.*, 247:209–230, 2013.

[29] J.H. Bramble and J.E. Pasciak. A note on the existence and uniqueness of solutions of frequency domain elastic wave problems: A priori estimates in h1. *Journal of Mathematical Analysis and Applications*, 345(1):396–404, 2008.

[30] R. Brunet, V. Dolean, and M. J Gander. Natural domain decomposition algorithms for the solution of time-harmonic elastic waves. *SIAM J. Sci. Comput.*, 42(5):A3313–A3339, 2020.

[31] O.P. Bruno and T. Yin. Regularized integral equation methods for elastic scattering problems in three dimensions. *J. Comput. Phys.*, 2020.

[32] P. Cance and Y. Capdeville. Validity of the acoustic approximation for elastic waves in heterogeneous media. *Geophysics*, 80 (4):T161–T173, 2015.

[33] J. M. Carcione. *Wave fields in real media: Wave propagation in anisotropic, anelastic, porous and electromagnetic media*. Elsevier, 2007.

[34] S. Chaillat and M. Bonnet. A new fast multipole formulation for the elastodynamic half-space green's tensor. *J. Comput. Phys.*, 258:787–808, 2014.

[35] S. Chaillat, M. Bonnet, and J.-F. Semblat. A Fast Multipole Method formulation for 3D elastodynamics in the frequency domain. *C.R. Mec.*, 335:709–714, 2007.

[36] S. Chaillat, M. Bonnet, and J.-F. Semblat. A multi-level fast multipole BEM for 3-D elastodynamics in the frequency domain. *Comput. Methods Appl. Mech. Eng.*, 197:4233–4249, 2008.

[37] S. Chaillat, L. Desiderio, and P. Ciarlet. Theory and implementation of $\mathcal{H}$-matrix based iterative and direct solvers for Helmholtz and elastodynamic oscillatory kernels. *J. Comput. Phys.*, September 2017.

[38] J. Chen and J-G. Zhao. Application of the nearly perfectly matched layer to seismic-wave propagation modeling in elastic anisotropic media. *Bull. Seismol. Soc. Am.*, 101:2866–2871, 12 2011.

[39] F. Collino. High order absorbing boundary conditions for wave propagation models. straight line boundary and corner cases. In R. Kleinman et al. (Eds.), editor, *Proc. 2nd Int. Conf. on Mathematical and Numerical Aspects of Wave Propagation*, pages pp. 161–171., Delaware, 1993. SIAM.

[40] F. Collino and C. Tsogka. Application of the perfectly matched absorbing layer model to the linear elastodynamic problem in anisotropic heterogeneous media. *Geophysics*, 66:294–307., 2001.

[41] S. Cummer. A simple, nearly perfectly matched layer for general electromagnetic media. *IEEE Microwave Wireless Compon. Lett.*, 13:128 – 130, 04 2003.

[42] M. Darbas and F. Le Louër. Well-conditioned boundary integral formulations for high-frequency elastic scattering problems in three dimensions. *Math. Methods Appl. Sci.*, 38(9):1705–1733, June 2015.

[43] E. Demaldent and S. Imperiale. Perfectly matched transmission problem with absorbing layers : application to anisotropic acoustics in convex polygonal domains. *Int. J. Numer. Methods Eng.*, 96(11):689–711, November 2013.

[44] B. Després. *Méthodes de décomposition de domaine pour les problemes de propagation d'ondes en régime ordinaire*. PhD thesis, PhD thesis, Université Paris IX Dauphine, 1991.

[45] A-S. Bonnet-Ben Dhia, S. Fliss, and Y. Tjandrawidjaja. Numerical analysis of the Half-Space Matching method with Robin traces on a convex polygonal scatterer. In *Maxwell's equations: Analysis and numerics*, volume 24 of *Radon Series on Computational and Applied Mathematics*. De Gruyter, May 2019.

[46] A.-S. Bonnet-Ben Dhia, S. Fliss, and A. Tonnoir. The halfspace matching method: a new method to solve scattering problem in infinite media. *J. Comput. Appl. Math.*, 338:44–68, 2018.

[47] J. Diaz and P. Joly. An analysis of higher order boundary conditions for the wave equation. *SIAM J. Appl. Math.*, 65(5):1547–1575 (electronic), 2005.

[48] J. Diaz and P. Joly. A time domain analysis of PML models in acoustics. *Comput. Methods Appl. Mech. Eng.*, 195(29-32):3820–3853, 2006.

[49] M. Dmitriev and V. Lisitsa. Application of m-pml absorbing boundary conditions to the numerical simulation of wave propagation in anisotropic media. part i: Reflection level. *Numer. Anal. Appl.*, 5:36–44, 01 2012.

[50] B. Engquist and A. Majda. Absorbing boundary conditions for numerical simulation of waves. *Proc. Natl Acad. Sci.*, 74(5):1765–1766, 1977.

[51] B. Engquist and A. Majda. Radiation boundary conditions for acoustic and elastic wave calculations. *Commun. Pure Appl. Math.*, 32:313–357, 1979.

[52] S. Fauqueux. *Eléments finis mixtes spectraux et couches absorbantes parfaitement adaptées pour la propagation d'ondes élastiques en régime transitoire*. Theses, ENSTA ParisTech, February 2003.

[53] S. Fliss. *Étude mathématique et numérique de la propagation des ondes dans des milieux périodiques localement perturbés*.

PhD thesis, PhD thesis, Ecole Polytechnique, 11 2009.

[54] S. Fliss and P. Joly. Exact boundary conditions for time-harmonic wave propagation in locally perturbed periodic media. *Appl. Numer. Math.*, 59(9):2155–2178, 2009.

[55] D. Givoli. *Numerical Methods for Problems in Infinite Domains*. Elsevier Science Limited, 1992.

[56] D. Givoli. High-order local non-reflecting boundary conditions: a review. *Wave Motion*, 39(4):319–326, 2004. New computational methods for wave propagation.

[57] D. Givoli. Computational absorbing boundaries. In B. Nolte (Eds.) S. Marburg, editor, *Computational Acoustics of Noise Propagation in Fluids*, chapter 5, pages pp. 145–166. Springer, Berlin, 2008.

[58] C. I. Goldstein. A finite element method for solving helmholtz type equations in waveguides and other unbounded domains. *Math. Comput.*, 39(160):309–324, 1982.

[59] T. Ha-Duong and P. Joly. On the stability analysis of boundary conditions for the wave equation by energy methods. part i: The homogeneous case. *Math. Comput.*, 62(206):539–563, 1994.

[60] T. Hagstrom. Radiation boundary conditions for the numerical simulation of waves. *Acta Numer.*, 8:47–106., 1999.

[61] T. Hagstrom, A. Mar-Or, and D. Givoli. High-order local absorbing conditions for the wave equation: Extensions and improvements. *J. Comput. Phys.*, 227(6):3322–3357, 2008.

[62] M. Halla, T. Hohage, L. Nannen, and J. Schöberl. Hardy space infinite elements for time harmonic wave equations with phase and group velocities of different signs. *Numerische Mathematik*, 133(1):103–139, 2016.

[63] L. Halpern, S. Petit-Bergez, and J. Rauch. The Analysis of Matched Layers. working paper or preprint, May 2011.

[64] I. Harari and U. Albocher. Studies of fe/pml for exterior problems of time-harmonic elastic waves. *Comput. Methods Appl. Mech. Eng.*, 195(29):3854–3879, 2006. Absorbing Boundary Conditions.

[65] J. Hesthaven. On the analysis and construction of perfectly matched layers for the linearized euler equations. *J. Comput. Phys.*, 142:129–147, 1998.

[66] R. L. Higdon. Numerical absorbing boundary conditions for the wave equation. *Math. Comput.*, 49:65–90, 1987.

[67] R. L. Higdon. Radiation boundary conditions for dispersive waves. *SIAM J. Numer. Anal.*, 31:64–100, 1987.

[68] R. L. Higdon. Radiation boundary conditions for elastic wave propagation. *SIAM J. Numer. Anal.*, 27:831–870, 1990.

[69] T. Hohage. Laplace domain methods for the construction of transparent boundary conditions for time-harmonic problems. In *Mathematical and numerical aspects of wave propagation—WAVES 2003*, pages 148–153. Springer, Berlin, 2003.

[70] T. Hohage, F. Schmidt, and L. Zschiedrich. Solving time-harmonic scattering problems based on the pole condition ii: Convergence of the pml method. *SIAM J. Math. Anal.*, 35(3):547–560, 2003.

[71] F. Q. Hu. On absorbing boundary conditions for linearized Euler equations by a perfectly matched layer. *J. Comput. Phys.*, 129(1):201–219, 1996.

[72] F. Q. Hu. A Stable, Perfectly Matched Layer for Linearized Euler Equations in Unsplit Physical Variables. *J. Comput. Phys.*, 173(2):455–480, 2001.

[73] J.B. Keller and M. J. Grote. Exact nonreflecting boundary condition for elastic waves. *SIAM J. Appl. Math.*, 60(3):803–819, 2000.

[74] M. Kitahara, K. Nakagawa, and J.D. Achenbach. Boundary-integral equation method for elastodynamic scattering by a compact inhomogeneity. *Comput. Mech.*, 5:129–144, 1989.

[75] D. Komatitsch and J. Tromp. A perfectly matched layer absorbing boundary condition for the second-order seismic wave equation. *Geophys. J. Int.*, 154(1):146–153, 2006.

[76] M. Lassas and E. Somersalo. On the existence and convergence of the solution of pml equations. *Computing*, 60(3):229–241, 1998.

[77] R. Martin, D. Komatitsch, and S. D. Gedney. A variational formulation of a stabilized unsplit convolutional perfectly matched layer for the isotropic or anisotropic seismic wave equation. *Computer Modeling in Engineering & Sciences*,

37(3):274–304, 2008.

[78] V. Mattesi, M. Darbas, and C. Geuzaine. A high-order absorbing boundary condition for 2d time-harmonic elastodynamic scattering problems. *Comput. Math. Appl.*, 77(6):1703–1721, 2019. 7th International Conference on Advanced Computational Methods in Engineering (ACOMEN 2017).

[79] L. Métivier, R. Brossier, S. Labbé, S. Operto, and J. Virieux. A robust absorbing layer method for anisotropic seismic wave modeling. *J. Comput. Phys.*, 279:218 – 240, December 2014.

[80] L. Métivier, R. Brossier, S. Labbé, S. Operto, and J. Virieux. SMART: dissipative absorbing layer technique for general elastodynamics equations. Application as S-waves filter in acoustic TI media. *Seismic Technology*, 11(4):1–14, October 2014.

[81] K. Meza-Fajardo and A. papageorgiou. A nonconvolutional, split-field, perfectly matched layer for wave propagation in isotropic and anisotropic elastic media: Stability analysis. *Bull. Seismol. Soc. Am.*, 98:1811–1836, 08 2008.

[82] A. Modave, V. Mattesi, and C. Geuzaine. High-order absorbing boundary conditions with edge and corner compatibility for the Helmholtz equation. In *ACOMEN 2017 - 7th International Conference on Advanced Computational Methods in Engineering*, Ghent, Belgium, September 2017.

[83] L. Nannen and M. Wess. Complex scaled infinite elements for exterior helmholtz problems, 2019.

[84] F. Nataf. A new approach to perfectly matched layers for the linearized Euler system. *J. Comput. Phys.*, 214(2):757–772, 2006.

[85] O. A. Oleïnik, A.S. Shamaev, and G.A. Yosifian. *Mathematical problems in elasticity and homogenization*. Elsevier, 2009.

[86] S. Operto, J. Virieux, A. Ribodetti, and E. Anderson. Finite-difference frequency-domain modeling of viscoacoustic wave propagation in 2d tilted transversely isotropic (tti) media. *Geophysics*, 74 (5):T75–T95, 2009.

[87] V. A. Osinov. Non-reflecting boundary conditions for plane waves in anisotropic elasticity and poroelasticity. *Acta Mech.*, 223(3):593–607, 2012.

[88] N. A. Petersson and B. Sjogreen. Wave propagation in anisotropic elastic materials and curvilinear coordinates using a summation-by-parts finite difference method. *J. Comput. Phys.*, 299:820–841, October 2015.

[89] D. Rabinovich, D. Givoli, J. Bielak, and T. Hagstrom. The double absorbing boundary method for elastodynamics in homogeneous and layered media. *Advanced Modeling and Simulation in Engineering Sciences*, 2, 12 2015.

[90] D. Rabinovich, D. Givoli, J. Bielak, and T. Hagstrom. The double absorbing boundary method for a class of anisotropic elastic media. *Comput. Methods Appl. Mech. Eng.*, 315, 11 2016.

[91] D. Rabinovich, S. Vigdergauz, D. Givoli, T. Hagstrom, and J. Bielak. Optimized first-order absorbing boundary conditions for anisotropic elastodynamics. *Comput. Methods Appl. Mech. Eng.*, 350:719–749, 2019.

[92] F. J. Rizzo, D. J. Shippy, and M. Rezayat. A boundary integral equation method for radiation and scattering of elastic waves in three dimensions. *Int. J. Numer. Methods Eng.*, 21(1):115–129, 1985.

[93] D. Royer and E. Dieulesaint. Onde élastiques dans les solides–tome 1: Propagation libre et guidée, 1996.

[94] E. A. Skelton, S. DM. Adams, and R.V. Craster. Guided elastic waves and perfectly matched layers. *Wave motion*, 44(7):573–592, 2007.

[95] Y. Tjandrawidjaja. *Some contributions to the analysis of the Half-Space Matching Method for scattering problems and extension to 3D elastic plates*. PhD thesis, ENSTA PARIS UNIVERSITÉ PARIS SACLAY, 12 2019.

[96] A. Tonnoir. *Conditions transparentes pour la diffraction d'ondes en milieu élastique anisotrope*. PhD thesis, Thèse de l'Ecole Polytechnique, 2015.

[97] G. Uhlmann and J-N. Wang. Unique continuation property for the elasticity with general residual stress. *Inverse Prob. Imaging*, 3(2):309–317, 2009.

[98] A. Zarmi and E. Turkel. A general approach for high order absorbing boundary conditions for the Helmholtz equation. *J. Comput. Phys.*, 242:387–404, June 2013.

[99] Z. Zhang, W. Zhang, and X. Chen. Complex frequency-shifted multi-axial perfectly matched layer for elastic wave modelling on curvilinear grids. *Geophys. J. Int.*, 198(1):140–153, 04 2014.